Postprint of: Kotov V., Bragov A., Balandin V., Igumnov L., Lomunov A., Eremeev V., Cazzani A., Cavity-expansion approximation for projectile impact and penetration into sand// CONTINUUM MECHANICS AND THERMODYNAMICS (2022), pp.1-27

V. L. Kotov · A. M. Bragov · V. V. Balandin · L. A. Igumnov · A. K. Lomunov · V. A. Eremeyev · A. Cazzani

Cavity-expansion approximation for projectile impact and penetration into sand

Abstract A one-dimensional problem of a spherical cavity expanding at a constant velocity from zero initial radius in an infinite granular medium, which has the first-kind self-similar solution, is considered. We are solving this dynamic spherical cavity-expansion problem to model rigid spheres penetrating into a granular media. Elastic–plastic deformation of the granular media is described in a barotropic approximation, using the high-pressure equation of state and Mohr–Coulomb Tresca's limit yield criterion. The medium is assumed to be incompressible behind the shock wave front propagating through the unperturbed medium. The problem in this formulation was solved analytically. Besides, a generalized solution of the problem was obtained numerically, which involves transition of a continuous elastic–plastic wave into a plastic shock wave when pressure grows with the cavity expansion velocity. The comparison of the analytical and numerical solutions shows that a linearized analytical solution is a good approximation of the pressure along the boundary of the cavity as a function of its expansion, except for low velocities. The linearized rigid plastic solution can be used

V. L. Kotov · A. M. Bragov · V. V. Balandin · L. A. Igumnov (✉) · A. K. Lomunov · V. A. Eremeyev
National Research Lobachevsky State University of Nizhny Novgorod, 23 Prospekt Gagarina (Gagarin Avenue) BLDG 6, 603950 Nizhny Novgorod, Russian Federation
E-mail: igumnov@mech.unn.ru

V. L. Kotov
E-mail: vkotov@inbox.ru

A. M. Bragov
E-mail: bragov@mech.unn.ru

V. V. Balandin
E-mail: balandin@mech.unn.ru

A. K. Lomunov
E-mail: lomunov@mech.unn.ru

V. A. Eremeyev
E-mail: eremeyev.victor@gmail.com

V. A. Eremeyev
Gdansk University of Technology, ul Narutowica, 11/12, 80-233 Gdansk, Poland

A. Cazzani
3University of Cagliari, DICAAR, 2, via Marengo, I-09123 Cagliari, Italy
E-mail: antonio.cazzani@unica.it

for analyzing resistance to a rigid sphere that penetrates into the granular media. The computational results are compared with known experimental relations for resistance to spherical projectiles penetrating dry and water-saturated sand. Good agreement between the numerical and experimental results is obtained without any correction factors.

Keywords Shock adiabat · Impact · Spherical projectile · Granular media · Sand · Dynamic cavity expansion

1 Introduction

The dynamic spherical cavity-expansion problem is a classical problem of mechanics of deformable solids. There exist many formulations of this problem differing in: (a) the way compressibility of the material is accounted for—linearly compressible media [1], incompressible media or media with limited ultimate strain [2,3]; b) the assumed yield criterion—Tresca [1,4], Mohr–Coulomb [2], Mohr–Coulomb with Tresca's limit [3]. There is a solution of the problem obtained using Drucker–Prager's model and the non-associated yield law [5]. For brittle media (ice, ceramics, concrete), the notion of the material failure zone is introduced [1,6]. There also exists an improved formulation of the problem, based on accounting for the dependence of the material properties on strain rate [7,8].

Papers [9–11] give approximations of cavity wall pressure as a function of its expansion taking into account the induced variation of mechanical properties of the material as well as parametric analysis of the obtained solutions. Alongside with dynamic formulations, static formulations of the problem are also considered [12], which are especially popular in soil mechanics [13–15]. Analytical solutions have been obtained for an incompressible elastic–plastic medium, using different types of yield criterion; for compressible media, some effective numerical algorithms [1] were proposed, based on the iterative method of numerical analysis of a boundary-value problem for a system of two first-order ordinary differential equations, which makes it possible to obtain an exact solution of the problem for the equation of state of a medium with nonlinear relationships [16,17].

Along with numerical solutions of the spherical cavity expansion problem, a new solution is given in [18] based on the analysis of the dimensionless cavity expansion rate for the model of a compressible von Mises medium with account for strain hardening. In [18], it is also postulated that most of the numerical and analytical solutions were obtained at moderate cavity expansion rates, while at higher radial expansion rates, a new plastic shock wave is possible to appear. In [19], the solution of the equations that includes the corresponding jump conditions through the shock wave was obtained. The technique [19] was elaborated on the problem of cavity expansion due to constant internal pressure under remote tension or compression focused on the porosity of the material at large deformations [20].

The dynamic spherical cavity-expansion problem has numerous applications in impact dynamics. In [1], it has been proposed the spherical cavity-expansion (SCE) approximation. From SCE approximation, every point on the lateral surface of the projectile is identified with the radial stress acting at the surface of a spherical cavity expanding at a constant velocity in an infinite medium starting from a zero initial radius. SCE approximation is extensively used in analyzing problems of impact and penetration into continua [21–25]. Analytic solutions of the problem of a spherical cavity expanding in an incompressible elastic–plastic medium [4,26–28] using SCE approximation are used in evaluating resistance forces and depths of penetration of rigid and deformable strikers into metals, concrete and soils. It was noticed [28] that incompressibility when accounted for in metals at impact velocities up to 1 km/s produces insignificant effects. This problem is still of scientific interest, as it is manifested in discussions [29–31] and [32–34].

The application of the approach based on solving the spherical cavity-expansion problem in the dynamics of geological materials is presented in [1,3,35,36]. Along with these works, an analysis of penetration of rigid and deformable projectiles at an angle to free surface soil, involving curvilinear motion trajectories, [37,38] can be noticed. An experimental–computational analysis of projectiles with flat, conical and hemispherical heads penetrating dry and water-saturated sand is presented in [39–44].

Generally, it can be noticed that the analysis of the cavity expansion problem and the methods of evaluating loads acting on the penetrator are well developed. Accounting for nonlinear material properties, when analyzing problems of penetration into compressible elastic–plastic media, poses no problem in numerically analyzing the cavity problem either.

One special feature in the deformation of soft soils is the necessity to account for both continuous elastic–plastic and shock waves. The presence of spherical shock waves in sandy and clayey soils, as well as the

dependence of the shock wave velocity on the pressure at its front, was shown experimentally [45–49]. It has to be noticed that the existing solutions of the cavity expansion problem do not account for the possible formation of a shock wave propagating through the unperturbed space.

The present article describes a formulation and analysis of a spherical cavity expansion problem, which can be applied for evaluating the force resisting a rigid penetrator in sandy soil. The hydrostatic pressure and deviatoric stress are defined by a high pressure equation of state and a Mohr–Coulomb pressure-dependent shear failure envelope with a Tresca's limit yield criterion. The numerically obtained generalized solution assumes the existence of an elastic region at subsonic propagation velocities of the elastic–plastic interface and the formation of a single plastic shock wave at supersonic velocities. In the assumption of incompressibility of the medium behind the shock wave front, an analytical solution of the problem has been obtained. This solution is similar to the earlier obtained rigid–plastic solution [1] of the cylindrical cavity expansion problem, where it was shown that the use of a rigid–plastic solution theoretically leads to overestimation of resistance to penetration. It should be noticed, however, that the approach itself, based on using the analysis of the cavity expansion problem in impact dynamics, is approximate; a solution is considered preferable, judging by its results in comparison with the experimental data. By comparing the experimental and numerical data, the authors have demonstrated that the model of a rigid penetrator in soil, using a simple linearized analytical rigid–plastic model, has a scope of applicability which is comparable with models based on numerically analyzing the cavity expansion problem.

2 Experimental methods for studying the behavior of sand under shock loading

Experimental studies of soil media have been carried out in the dynamic testing laboratory of the Research Institute for Mechanics of Lobachevsky State University of Nizhny Novgorod under the guidance of prof. Bragov A.M. since 1980. Two original setups developed on the basis of 57 mm gas cannon were used in the experiments. The shock compressibility of sand (shock adiabat) was determined in plane-wave experiments. The penetration resistance forces were measured in inverted experiments using a measuring bar.

2.1 The method of constructing a shock adiabat

To study the dynamic compressibility of granular media, the reflection method [50], also called the impedance match technique, is used. In the method, the accelerated striker plate hits a specimen not directly, but through a screening plate. The shock adiabats of the materials of the striker and the screen must be known. Besides, the initial density of the studied material must be determined in advance. The measured parameters are shockwave front velocity U_S and striker velocity U_0, which (for equal properties of the striker and of the target) is equal to the double of particle mass velocity υ in the target (Fig. 1). The parameters in the shock wave are related through the Rankine–Hugoniot conservation laws with thermodynamic consideration. These parameters in the shock wave are related through the pulse conservation laws with the thermal dynamic characteristics—pressure $P = \rho_0 U_s \upsilon$ and impact compression density $\rho_s = \rho_0 U_s \big/ (U_s - \upsilon)$; ρ_0 is the original density. Measuring the two independent parameters (namely U_s and υ) makes it possible to determine the shock adiabat of the soil.

Figure 2 shows schematically an experimental stand used for realizing the methodology of constructing a shock adiabat using the reflection method.

An 8-mm-thick soil layer was placed between two plates made of an aluminum alloy. Compression waves were induced in a 5-mm-thick screening plate struck by a projectile (impactor) which has been accelerated using a 57-mm-caliber gas gun. As a result, a plane compression wave was formed both in the screening plate and in the specimen. The impact velocity varied in the range 100–500 m/s and was measured using electro-contact speedometers with an accuracy of up to 2%. The thicknesses of the plate striker, of the screening plate and of the specimen were chosen such that unloading waves from the free surfaces could not distort the picture of one-dimensional strain in the compression wave. Changing impact velocity V and propagation velocity U_s of the compression wave through the specimen in combination with known adiabats of the striker and the screening plate makes it possible to determine the point of the shock adiabat of the studied medium.

A 57-mm-caliber gas gun was used to apply the loading. The propagation velocity of the compressive wave in the specimen was measured with two dielectric pressure gauges located on the specimen surfaces. Each gauge consisted of two 0.05-mm-thick 20-mm-diameter current collectors made of copper foil and a 0.05-mm-thick sensitive element of dielectric (PET film). The total thickness of the gauge is 0.2 mm. When a plane wave travels through the specimen within the gauges, the compression pulse induces electric signals on the armature

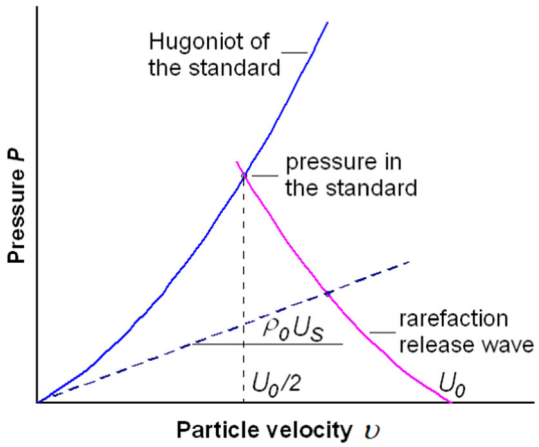

Fig. 1 A scheme for determining the shock adiabat of granular media by using the impedance match technique

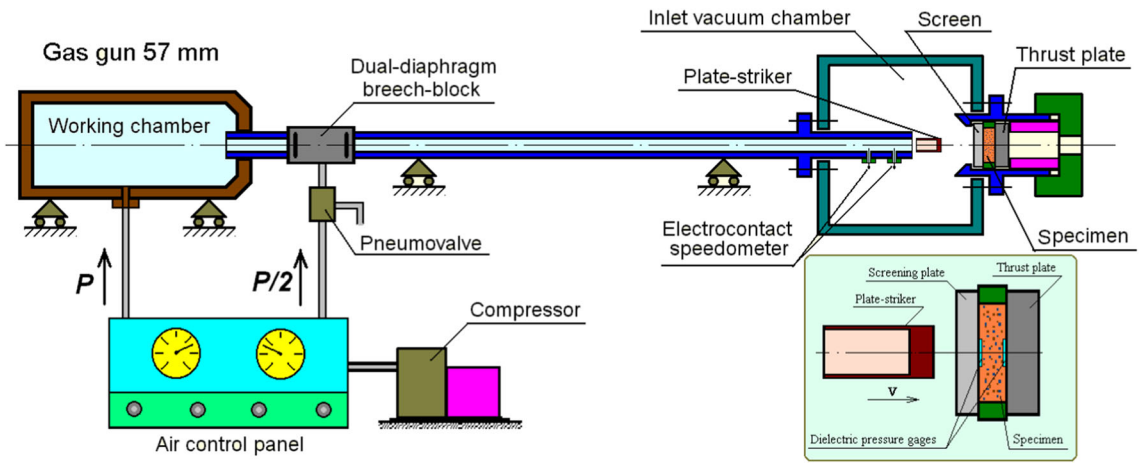

Fig. 2 The experimental configuration (schematically)

of the gauges, which are registered in the memory of the oscillograph. The compression wave propagation velocity through the soil specimen can be determined based on the distance between the gauges and the traveling time of the pressure pulses relative to each other. In testing soil materials in conditions of shockwave loading, special attention was paid to inducing a plane wave with one-dimensional strain. Inducing a plane wave is possible provided that warping is minimized, when the striker hits the screening plate. Accordingly, the parallelism of the planes of the specimen and the striker was thoroughly checked before each test.

To synchronize the time base of the oscillograph with the beginning of the process, an electro-contact gauge, in the form of a 0.05-mm-thick copper foil stripe cemented on a 0.05-mm-thick insulating film, was secured on the surface of the screening plate impacted by the plate striker. When the projectile hit the plate, the gauge short-circuited and triggered the oscillograph to start recording.

The analysis of the measurements and of processing the test data in the plane-wave experiments showed that the inaccuracies in determining the parameters of shock adiabats are less than 7% [51].

Experimenting with different impact velocities makes it possible to obtain several points of the shock adiabat of the material.

2.2 The inverse experiment technique using the measuring bar

The methodology of measuring the force resisting penetration of a projectile into sand using a measuring bar [44] is schematically shown in Fig. 3.

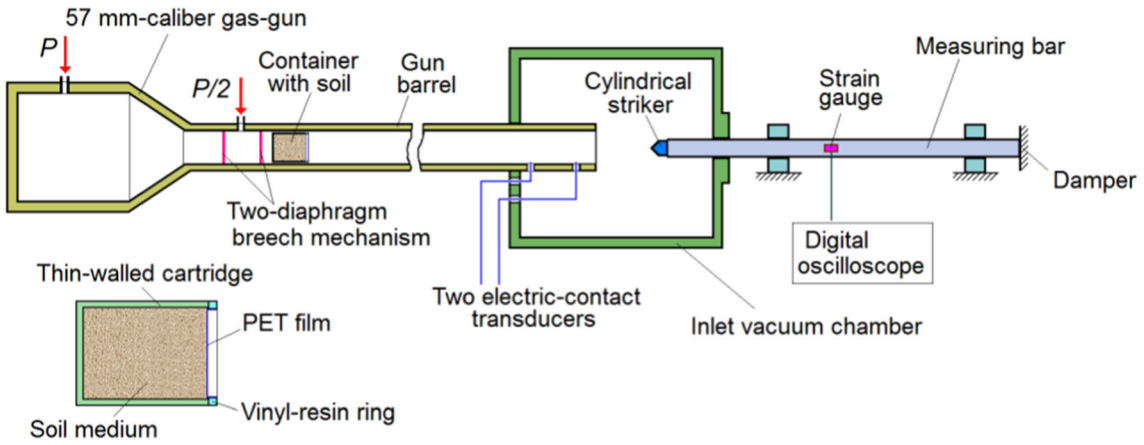

Fig. 3 Schematic representation of the setup for measuring forces resisting penetration in the inverse experiment

A container filled with soil (sand) is accelerated up to the required velocities and impacted against a stationary striker fixed on a measuring bar. The impact velocity and the material properties are to be such that no plastic strains should occur in the bar. An elastic strain pulse $\varepsilon(t)$ is formed in the bar. Registering this pulse on the surface of the bar makes it possible to determine the force F, acting on the striker upon its interaction with the medium, according to the known relation $F(t) = E\varepsilon(t) S_0$, where E is the elastic modulus of the bar and S_0 is its cross section area.

Thus, in this method, the task of measuring the forces is considerably simplified and reduced to registering an elastic strain pulse in the bar, using strain gauges. The setup implementing this method is schematically depicted in Fig. 3. In the present version of the inverse experiment, a soil container is accelerated using a 57-mm-caliber gas gun with a two-diaphragm breech mechanism, which makes it possible to provide stable and readily controlled impact velocities in the range from 50 to 500 m/s, using air compressed up to 15 MPa, and up to ~1000 m/s, when using compressed helium.

The container is a thin-walled cartridge, filled with soil. To prevent the soil from spilling in the process of preparation of the experiment and during acceleration of the container after the container entirely leaves the barrel's muzzle, the front end of the container is sealed with 0.01-mm-thick PET film. The film is fixed and secured against the surface of the soil with a vinyl-resin ring.

The impact velocity of the container was determined using two electric-contact transducers located in the orifices of the barrel, made in the vicinity of the muzzle. A 1.5-m-long 20-mm-diameter steel rod with yield strength larger than 2000 MPa was used as a measuring bar. The steel measuring bar had density $\rho = 8050$ kg/m^3, Young's modulus $E = 186$ GPa. One of the ends of the measuring bar has a threaded orifice housing a cylindrical striker with a head of appropriate geometry. The bar is located at a certain distance from the barrel muzzle, so that the impact occurs immediately after the container entirely leaves the barrel. The stand on which the bar is located has adjusting supports, which are used to provide axisymmetric interaction. The rear end of the bar rests against a special damper, preventing it from displacing and damping the impact energy. Impact takes place inside a vacuum chamber, to which the gun barrel is connected, and into which the measuring bar with its head is introduced. The cylindrical part of the heads was 19.8 mm in diameter, with the radius of the hemisphere equal to 10 mm, and were made of steel with a yield strength larger than 1800 MPa.

2.3 The conditions of the experiments

For the inverse tests, cylindrical containers made of aluminum alloy were used, which had the following dimensions: outer diameter 56.8 mm, inside diameter 54 mm, bottom thickness 2 mm, filling depth 65 mm. To prevent sand from strewing out during the test, the sand surface in the container was fixed with a 0.01-mm-thickness PET film.

Both experiments were conducted with dry and water saturated (wet) sandy mixture of a natural composition, from which particles larger than 1 mm and smaller than 0.1 mm had been removed. The particle size distribution of dry sand mixture is presented in Table 1.

Table 1 Particle size distribution of the sand used in experiments

Mean particle diameter (mm)	The granules lie in the range between the size value shown in the given column and the size value in the column immediately to the left of that.					
	0.63	0.4	0.315	0.2	0.16	0.1
% finer by mass	5.0	21.5	13.2	38.8	11.6	9.9

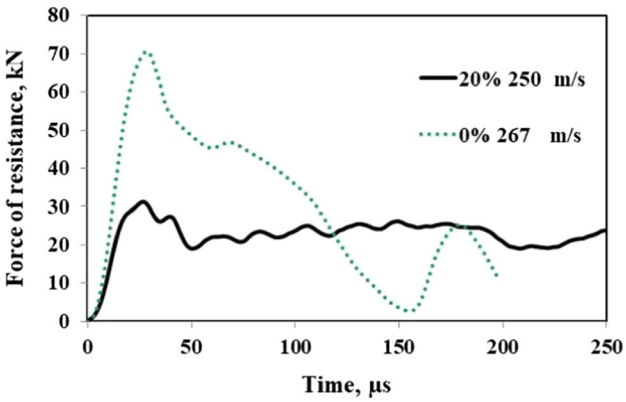

Fig. 4 Dependences of the force resisting to penetration into dry (0%) and water-saturated (20%) sand for a hemisphere at close impact velocities ($\sim 250 - -260$ m/c)

The dry sand filled into the container was compacted layer-by-layer until reaching an average density of about 1750± 50 kg/m^3. In the tests of water-saturated sand, the containers filled with dry sand were poured with a certain amount of water until the sand was completely saturated. Further saturation resulted in the formation of a water layer over the surface of the sand, so the excess water was poured off. The containers were weighed again to determine the density of the water-saturated sand and its moisture content relative to its initial density. The average density of the water-saturated (wet) natural mixture was 2080± 50 kg/m^3.

Figure 4 shows the experimental dependences of the force resisting to penetration into dry and water-saturated sand of a projectile with a hemispherical head. The initial section of penetration of hemispherical strikers into a sand target is characterized by a rapid increase in the force resisting to penetration. Experiments have shown that the maximum values of the resistance force for different impact velocities are achieved in a time of 25–50 μs (with increasing impact velocity, the time to reach the maximum decreases). It should be noted that for dry sand, the resistance force reaches its maximum value when the striker is deepened by 5–6 mm, i.e., by 0.5 –0.6 radius. Further, a separation of the flow from the surface of the hemisphere occurs and cavity formation around the striker takes place, as a result, the resistance force decreases with further deepening to a quasi-stationary value. A characteristic feature of the obtained "resistance force—time" dependences for water-saturated sand is a shorter time for the resistance force to reach its maximum as compared to a hemispherical impactor penetrating into dry sand.

Based on these results, the dependences of the maximum values of the force on the speed were determined. The error in determining the maximum resistance force was no more than 10%.

3 Analyzing the problem of a spherical cavity expanding in a soft soil

3.1 Analytical solution in the assumption of incompressibility of the medium behind the shock wave front

3.1.1 Formulating an initial boundary-value problem for a system of partial differential equations

A mathematical model of a granular medium is described by a system of differential equations: continuity equation and equation of motion following from the conservation of mass and the balance of momentum,

which in spherical Eulerian coordinates can be written as:

$$\rho\left(\frac{\partial \upsilon}{\partial r}+2\frac{\upsilon}{r}\right)=-\left(\frac{\partial \rho}{\partial t}+\upsilon\frac{\partial \rho}{\partial r}\right),$$
$$\frac{\partial \sigma_r}{\partial r}+2\frac{(\sigma_r-\sigma_\theta)}{r}=-\rho\left(\frac{\partial \upsilon}{\partial t}+\upsilon\frac{\partial \upsilon}{\partial r}\right), \tag{1}$$

where ρ is the density in the deformed configuration, υ the radial particle velocity measured positive outward, and σ_r, σ_θ the radial and circumferential components of Cauchy stress tensor measured positive in compression, r is the radial Eulerian coordinate, and t is time.

The granular medium is described by the equation of state and the yield criterion:

$$\sigma_r = f_1(\theta),\ \sigma_r-\sigma_\theta = f_2(\theta) \tag{2}$$

where $\theta = 1-\rho_0/\rho$ is volumetric strain, and ρ_0 is the original density. Functions $f_1$and f_2 are determined from the experiments.

Along the boundary of a cavity whose radius is $R_0 = Vt$, expanding from zero radius ($R_0|_{t=0} = 0$), the velocity V is assigned, the outer surface of spherical layer R_∞ is free from stresses, and at the initial time both velocity and stresses in the medium are equal to zero:

$$\upsilon(R_0,t)=V,\ \sigma_r(R_\infty,t)=0,\ \upsilon(r,0)=\sigma_r(r,0)=0. \tag{3}$$

The solution of the problem is constructed in the plastic yield region bounded by the cavity radius $r = Vt$ and $r = ct$, when $c$is the plastic interface velocity.

3.1.2 Formulating a boundary-value problem for a system of first-order partial differential equations

Following [1–9], self-similar variable $\xi = r/ct$ is used in the solution of the problem. The partial derivatives in time and space are defined as follows:

$$\frac{\partial \upsilon}{\partial r}=\frac{d\upsilon}{d\xi}\frac{\partial \xi}{\partial r}=\frac{1}{ct}\frac{d\upsilon}{d\xi},\ \frac{\partial \upsilon}{\partial t}=\frac{d\upsilon}{d\xi}\frac{\partial \xi}{\partial t}=-\frac{\xi}{t}\frac{d\upsilon}{d\xi},\ \frac{\partial \sigma_r}{\partial r}=\frac{1}{ct}\frac{d\sigma_r}{d\xi},\ \frac{\partial \sigma_r}{\partial t}=-\frac{\xi}{t}\frac{d\sigma_r}{d\xi}.$$

The system of partial differential equations (1) is transformed into a system of ordinary differential equations (ODE), assuming a time $t > 0$:

$$\frac{1}{c}\frac{d\upsilon}{d\xi}+2\frac{\upsilon}{\xi c}=\frac{(\xi-\upsilon/c)}{(1-\theta)}\frac{d\theta}{d\xi},$$
$$\frac{1}{\rho c^2}\frac{d\sigma_r}{d\xi}+2\frac{f_2}{\xi\rho c^2}=(\xi-\upsilon/c)\frac{1}{c}\frac{d\upsilon}{d\xi}. \tag{4}$$

For $\xi = 1$, Rankine–Hugoniot's jump conditions are used on the shock wave:

$$[\rho]c-[\rho\upsilon]=0,\ [\rho\upsilon]c-\left[\rho\upsilon^2+\sigma_r\right]=0. \tag{5}$$

In (5), square brackets designate difference of the values to the left and to the right of the discontinuity, and c is the propagation velocity of the discontinuity. The values to the left and to the right of the discontinuity will be designated as ρ_s, υ, σ and $\rho_0, \upsilon_0, \sigma_0$, respectively.

In view of its smallness the elastic precursor in a granular medium can be neglected. Then, assuming $\upsilon_0 = \sigma_0 = 0$, one has $(\rho_s-\rho_0)c = \rho_s\upsilon$, $\rho_s\upsilon c = \rho_s\upsilon^2+\sigma$, or $1-\rho_0/\rho_s \equiv \theta_s = \upsilon/c$, $\upsilon/c-(\upsilon/c)^2 = \sigma/\rho_s c^2$.

It is also assumed that, at high cavity expansion velocities, the compressibility of the granular medium is low; then system (4) is considered in the assumption of incompressibility of the medium, i.e., when equalities $d\theta/d\xi = 0$ or $\theta = const$ do hold.

In equations (4), the value of the volumetric strain is taken to be $\theta \equiv \theta_s$ and $\rho \equiv \rho_s$. The fact that density retains its value ρ_s on the shock wave amounts to the assumption of incompressibility of the medium behind the shock wave front. Values of ρ_s and θ_s are determined for every value of cavity expansion velocity.

Having chosen $U = \upsilon/c$ and $S_r = \sigma_r/\rho_s c^2$ as dimensionless variables, one gets the following system of ODE (the prime designates differentiation with respect to ξ)

$$U' + 2\frac{U}{\xi} = 0,\ S_r' + 2\frac{\tilde{f}_2}{\xi} = (\xi - U)\,U',\ \varepsilon < \xi < 1 \tag{6}$$

and boundary conditions

$$\begin{aligned} &U(\xi = \varepsilon) = \varepsilon, \\ &U(\xi = 1) = \theta_s,\ S_r(\xi = 1) = U - U^2 = \theta_s - \theta_s^2, \end{aligned} \tag{7}$$

where the following definitions are introduced: $\varepsilon = V/c$ is the dimensionless spherical cavity-expansion velocity, $\tilde{f}_2 = f_2/\rho_s c^2$ is a dimensionless function in the plasticity condition.

3.1.3 Solution of the boundary-value problem for a system of ODE with Mohr–Coulomb yield criterion

To solve the boundary-value problem for a system of two first-order ordinary differential Eqs., (6), (7), it is necessary to provide functions $f_1$and f_2 of the equation of state and yield criterion of the medium.

Experiments [48,49] indicate that dynamic compressibility of soil media is characterized by a shock adiabat in the form of a linear relation:

$$U_s = C_0 + s\upsilon, \tag{8}$$

Here, C_0 is defined as the bulk sound speed, and $s$is defined as the slope of the U_s versus υ relation and is obtained from the first term in the expansion in Eqs. (4) of [52].

Relations (8) were obtained experimentally in shock-wave experiments for the conditions of uniaxial strain. In the present formulation of the spherical cavity expansion problem, the shockwave velocity and the plastic wave velocity are taken to be equal to $U_s \equiv c$. This is another simplifying assumption, mentioned earlier in [1].

Substituting relation (8) into Rankine–Hugoniot's Eq. (5), one obtains $\upsilon = \theta c$, $\sigma_r = \rho_0 \upsilon c = \rho_0 \theta c^2$; relation (8) will become $c = C_0 + s\theta c$, $c = C_0/(1 - s\theta)$. The final hydrostatic form of the relation between stress $\sigma_r = \rho_0 \upsilon c = \rho_0 \theta c^2$ and volumetric strain θ will be $f_1(\theta) \equiv \rho_0 C_0^2 \theta\,(1 - s\theta)^{-2}$ [48], which has been used earlier in computations [53,54]. In this formulation, parameter s characterizes compression strength of the soil. The barotropic approximation applied to soil media is justified by the fact that, at pressures up to 10 GPa, the relative thermal volumetric expansion is an order of magnitude smaller than the total relative change of the volume.

Taking account of conditions (8) on the shock wave, boundary conditions (7) can be rewritten as follows:

$$U(\xi = \varepsilon) = \varepsilon,\ U(\xi = 1) = \left(1 - C_0/c\right)/s. \tag{9}$$

The first equation of system Eq. (6) is an equation with branching variables $dU/U = -2d\xi/\xi$, the solution of which yields $U = c_1/\xi^2$. Constant c_1 is determined from the first boundary condition in (9) as $c_1 = \varepsilon^3$, and the dimensionless velocity has the following form:

$$U = \varepsilon^3/\xi^2. \tag{10}$$

To determine the unknown value ε, taking into account the second boundary condition in relations (9) $\varepsilon^3 = \left(1 - C_0/c\right)/s = \left(1 - C_0 V/Vc\right)/s = \left(1 - \varepsilon/M\right)/s$, the following cubic equation is obtained:

$$\varepsilon^3 + \frac{\varepsilon}{sM} - \frac{1}{s} = 0, \tag{11}$$

where $M = V/C_0$. The coefficients in Eq. (11) depend only on the parameters of the shock adiabat of the medium C_0, s and cavity expansion velocity V.

An exact solution of Eq. (11) according to Cardano's formula has the following form:

$$\varepsilon = \sqrt[3]{1/(2s) + q} + \sqrt[3]{1/(2s) - q}, \tag{12a}$$

where the definition $q = \sqrt{(2s)^{-2} + (3sM)^{-3}}$ has been introduced.

A linear approximation to ε, which follows from Eq. (1), when using Taylor's expansion $\varepsilon = \frac{1}{\sqrt[3]{s}}\left(1 + \left(-\frac{\varepsilon}{M}\right)\right)^{1/3} \approx \frac{1}{\sqrt[3]{s}}\left(1 - \frac{\varepsilon}{3M}\right)$, yields

$$\varepsilon \approx 3M\big/\left(1 + 3M\sqrt[3]{s}\right). \tag{12b}$$

Using the definition $\varepsilon = V\big/c$, one obtains

$$c = V\left(\sqrt[3]{1\big/(2s) + q} + \sqrt[3]{1\big/(2s) - q}\right)^{-1}, \tag{13a}$$

$$c \approx \sqrt[3]{s}V + C_0/3. \tag{13b}$$

Earlier, a solution of the form of (13a) was obtained in the cylindrical cavity expansion problem [1].

It is further assumed that the plasticity criterion of the medium is described by Mohr–Coulomb's law $f_2 \equiv \tau + \kappa p$, where τ is cohesion, κ is internal friction coefficient, $p = (\sigma_r + 2\sigma_\theta)\big/3$ is hydrostatic pressure.

The second equation of system (6) and the second boundary condition in (7) when taking into account solution (10) and the yield criterion will be written as:

$$S_r' + 2\frac{T_0 + \mu S_r}{\xi} = -2\left(\xi - \frac{\varepsilon^3}{\xi^2}\right)\frac{\varepsilon^3}{\xi^3} = -2\frac{\varepsilon^3}{\xi^2} + 2\frac{\varepsilon^6}{\xi^5},\ S_r\,(\xi = 1) = \varepsilon^3 - \varepsilon^6, \tag{14}$$

where $T_0 = \tau_0\big/\rho_s c^2$, $\tau_0 = 3\tau\big/(3 + 2\kappa)$, $\mu = 3\kappa\big/(3 + 2\kappa)$.

Transferring the terms containing S_r in Eq. (14) into the left-hand side and the rest of the terms into the right-hand side, and multiplying the left-hand and the right-hand sides of the equation by $\xi^{2\mu}$:

$$\left(S_r' + 2\frac{\mu S_r}{\xi}\right)\xi^{2\mu} = \left(-2\frac{T_0}{\xi} - 2\frac{\varepsilon^3}{\xi^2} + 2\frac{\varepsilon^6}{\xi^5}\right)\xi^{2\mu},$$

one obtains, after some transformations, an equation with branching variables, $d\left(S_r\xi^{2\mu}\right) = \left(-2T\xi^{2\mu-1} - 2\varepsilon^3\xi^{2\mu-2} + 2\varepsilon^6\xi^{2\mu-5}\right)d\xi$, the solution of which depends on the arbitrary variable c_2

$$S_r = -\frac{T_0}{\mu} - 2\frac{\varepsilon^3}{(2\mu - 1)\,\xi} + \frac{\varepsilon^6}{(\mu - 2)\,\xi^4} + c_2\xi^{-2\mu}.$$

Taking into account boundary conditions (14), the dimensionless stress takes the form:

$$S_r\,(\xi) = -\frac{T_0}{\mu} - 2\frac{\varepsilon^3}{(2\mu - 1)\,\xi} + \frac{\varepsilon^6}{(\mu - 2)\,\xi^4} + \left(\frac{T_0}{\mu} + 2\frac{\varepsilon^3}{(2\mu - 1)} - \frac{\varepsilon^6}{(\mu - 2)} + \varepsilon^3 - \varepsilon^6\right)\xi^{-2\mu}. \tag{15a}$$

Equation (15a) is not defined for μ =0 and μ =0.5. In these cases, a solution can be obtained by passing to the limit in (15a) for μtending to 0 and 0.5, respectively

$$S_r\,(\xi) = -2T_0\ln\xi - \varepsilon^3\left(1 - \frac{2}{\xi}\right) - \frac{\varepsilon^6}{2}\left(1 + \frac{1}{\xi^4}\right),\ \mu = 0, \tag{15b}$$

$$S_r\,(\xi) = -2T_0\left(1 - \frac{1}{\varepsilon}\right) - \varepsilon^3\left(2\frac{\ln\xi}{\xi} - \frac{1}{\xi}\right) - \frac{\varepsilon^6}{3}\left(\frac{1}{\xi} + \frac{2}{\xi^4}\right),\ \mu = 0.5. \tag{15c}$$

In a dimensional form, the stress as a function of the self-similar variable has the following form:

$$\sigma_r\,(\xi) = \tau_0\left(\frac{\xi^{-2\mu} - 1}{\mu}\right) + \frac{\rho_0 V^2\varepsilon}{1 - \varepsilon^3}\left(\frac{2}{(2\mu - 1)}\left(\frac{\xi^{-2\mu+1} - 1}{\xi}\right) + \frac{\varepsilon^3}{(\mu - 2)}\left(\frac{1 - \xi^{-2\mu+4}}{\xi^4}\right) + \left(1 - \varepsilon^3\right)\xi^{-2\mu}\right) \tag{16}$$

Equations (16) were derived using the equality $\rho_s = \rho_0\big/\left(1 - \varepsilon^3\right)$.

The dimensionless stress on the cavity wall ($\sigma_C \equiv \sigma_r\,(\xi = \varepsilon)$) is defined as:

$$S = T_0\left(\frac{\varepsilon^{-2\mu}-1}{\mu}\right) + \frac{3\varepsilon^2}{(2\mu-1)(\mu-2)} + \varepsilon^3\left(\frac{2}{(2\mu-1)} - \frac{\varepsilon^3}{(\mu-2)} + 1 - \varepsilon^3\right)\varepsilon^{-2\mu}.$$

In a dimensional form, the stress $\sigma_C \equiv \sigma_r\,(\xi = \varepsilon)$ on the boundary of the spherical cavity expanding at a velocity V, has the following form:

$$\sigma_C = \tau_0\left(\frac{\varepsilon^{-2\mu}-1}{\mu}\right) + \frac{\rho_0 V^2}{1-\varepsilon^3}\left(\frac{3}{(\mu-2)(2\mu-1)} + \frac{2\mu+1}{2\mu-1}\cdot\varepsilon^{1-2\mu} - \frac{\mu-1}{\mu-2}\cdot\varepsilon^{4-2\mu}\right), \quad (17a)$$

$$\sigma_C = -2\tau_0 \ln\varepsilon + \frac{\rho_0 V^2}{1-\varepsilon^3}\left(3/2 - \varepsilon - \varepsilon^4/2\right)., \mu = 0 \quad (17b)$$

$$\sigma_C = 2\tau_0\left(\varepsilon^{-1}-1\right) + \frac{\rho_0 V^2}{1-\varepsilon^3}\left(1/3 - 2\ln\varepsilon - \varepsilon^3/\right), \mu = 0.5 \quad (17c)$$

In Eqs. (2), (17), the value of ε is determined based on Eq. (12). The relations for stresses obtained by substituting Eqs. (12a) and (12b) are in what follows called *rigid–plastic* and *linearized rigid–plastic*, respectively. Thus, final relations have been obtained, which make it possible to determine the stress in a medium with Mohr–Coulomb's plasticity condition.

3.1.4 Solution of a boundary-value problem for a system of ODE with Mohr–Coulomb Tresca-limit yield criterion

Then, we consider the Mohr–Coulomb pressure-dependent shear strength taking into account the limitation of the maximum yield strength τ_M as supposed by Tresca-limit yield criterion.

Stress S_r monotonically decreases with the dimensionless coordinate ξ changing from ε to 1, i.e., the minimal stress value is achieved at ξ =1. The value of cavity expansion velocity V_M, at which $S_r\,(\xi = 1) = S_M$, is then determined (in which $S_M = (T_M - T_0)/\mu$ and $T_M = \tau_M/\rho_s c^2$).

From the Rankine–Hugoniot relations on the shock wave for ξ =1 it follows that $\sigma_r = \rho_0 c\upsilon = \rho_0 c^2\theta$. The values of shock wave velocity, volumetric strain and ε, corresponding to $V = V_M$, will be designated as c_M, θ_M and ε_M, respectively. To determine c_M, formula (13b) will be used, yielding

$$c_M = \sqrt[3]{s}V_M + C_0/3, \theta_M = \varepsilon_M^3 = \frac{V_M^3}{c_M^3}, \sigma_M = \rho_0 c_M^2\theta_M = \rho_0\frac{V_M^3}{c_M},$$

where $\sigma_M = (\tau_M - \tau_0)/\mu$. Then, to determine V_M, the following cubic equation is obtained:

$$\left(\frac{\tau_M - \tau_0}{\mu}\right)\left(\sqrt[3]{s}V_M + C_0/3\right) = \rho_0 V_M^3 \quad (18a)$$

In a similar way, the maximal stress value is achieved at $\xi = \varepsilon$. Symbol V_0 will designate the value of cavity expansion velocity, at which equalities $S_r\,(\xi = \varepsilon) = S_M$ or $\sigma_r\,(\xi = \varepsilon) = \sigma_M$ hold. Substituting value $V = V_0$ into Eq. (17), $\sigma_M = \sigma_r\,(\xi = \varepsilon)\big|_{V=V_0}$, the following nonlinear equation for determining V_0 is obtained:

$$\frac{\tau_M - \tau_0}{\mu} = \frac{\tau_0}{\mu}\left(1 - \varepsilon_0^{-2\mu}\right) + \frac{\rho_0 V_0^2}{1-\varepsilon_0^3}\left(\frac{3}{(\mu-2)(2\mu-1)} + \frac{2\mu+1}{2\mu-1}\cdot\varepsilon_0^{1-2\mu} - \frac{\mu-1}{\mu-2}\cdot\varepsilon_0^{4-2\mu}\right), \quad (18b)$$

where definitions $\varepsilon_0 = V_0/c_0$, $c_0 = \sqrt[3]{s}V_0 + C_0/3$ have been introduced.

For a cavity expansion velocity varying in the interval $V_0 < V < V_M$, it is necessary to find the value of the dimensionless coordinate $\xi = \xi_M$, at which the value of the dimensionless stress is $S_r\,(\xi = \xi_M) = S_M$.

Finally, the dimensionless stress will be defined as:

$$S_r(\xi) = \begin{cases} -\frac{T_0}{\mu} - 2\frac{\varepsilon^3}{(2\mu-1)\xi} + \frac{\varepsilon^6}{(\mu-2)\xi^4} + \\ + \left(\frac{T_0}{\mu} + 2\frac{\varepsilon^3}{(2\mu-1)} - \frac{\varepsilon^6}{(\mu-2)} + \varepsilon^3 - \varepsilon^6\right)\xi^{-2\mu}, & \begin{pmatrix} 0 < \varepsilon < \varepsilon_0, \\ \varepsilon \le \xi \le 1 \end{pmatrix} \cup \\ & \begin{pmatrix} \varepsilon_0 < \varepsilon < \varepsilon_M, \\ \xi_M \le \xi \le 1 \end{pmatrix}; \\ S_M + T_M \ln\left(\frac{\xi_M}{\xi}\right)^2 + 2\varepsilon^3\left(\frac{1}{\xi} - \frac{1}{\xi_M}\right) - \frac{\varepsilon^6}{2}\left(\frac{1}{\xi^4} - \frac{1}{\xi_M^4}\right), & \varepsilon_0 \le \varepsilon \le \varepsilon_M, \\ & \varepsilon \le \xi \le \xi_M; \\ -2T_M \ln\xi - \varepsilon^3\left(1 - \frac{2}{\xi}\right) - \frac{\varepsilon^6}{2}\left(1 + \frac{1}{\xi^4}\right), & \varepsilon > \varepsilon_M, \\ & \varepsilon \le \xi \le 1. \end{cases} \tag{19}$$

Dimensional stress along the cavity boundary $\sigma_C \equiv S_r(\xi = \varepsilon)\,\rho_s c^2$,

$$\sigma_r(V) = \begin{cases} \frac{\tau_0}{\mu}\left(\varepsilon^{-2\mu} - 1\right) + \frac{\rho_0 V^2}{1-\varepsilon^3}\left(\frac{3}{(\mu-2)(2\mu-1)} + \frac{2\mu+1}{2\mu-1}\cdot\varepsilon^{1-2\mu} - \frac{\mu-1}{\mu-2}\cdot\varepsilon^{4-2\mu}\right), & 0 < V < V_0; \\ \sigma_M + \tau_M \ln\left(\frac{\xi_M}{\varepsilon}\right)^2 + \frac{\rho_0 V^2}{1-\varepsilon^3}\left(\frac{3}{2} - \frac{2\varepsilon}{\xi_M} + \frac{\varepsilon^4}{2\xi_M^4}\right), & V_0 \le V \le V_M, \\ -2\tau_M \ln\varepsilon + \frac{\rho_0 V^2}{1-\varepsilon^3}\left(\frac{3}{2} - \varepsilon - \frac{\varepsilon^4}{2}\right), & V > V_M. \end{cases} \tag{20}$$

In Eqs. (6) and (7), the value of ε is determined in the same way, using Eq. (12). Thus, the final relations are obtained, which make it possible to determine the stress in a medium with Mohr–Coulomb Tresca-limit yield criterion.

3.2 Numerical solution of the problem in a complete formulation

3.2.1 Formulating an initial boundary-value problem for a system of partial differential equations

A mathematical model of a soil medium is described by differential equation system (1), which is closed by an invariant relation between pressure and volumetric strain:

$$p = f_3(\theta) \equiv K\theta + O\left(\varepsilon^2\right), \tag{21}$$

where K is the elastic bulk modulus (i.e., the modulus of volumetric compression).

It is assumed that in the region bounded by radii $R_0 = Vt$ and $r = ct$, the medium is plastically deformed, and c is the velocity of propagation of the plastic wave. In the adjacent region of elastic deformation, which is bounded by coordinate $r = c_e t$, the stress tensor components are related to strains by Hooke's law with elastic moduli K and G where $c_e = \sqrt{(K + 4G/3)/\rho_0}$ is the plane elastic wave propagation velocity, and G is the shear modulus.

A solution of a one-dimensional problem of spherical cavity expansion in the region of plastic deformation will be now constructed. In view of the spherical symmetry and of the fact that the first invariant of the deviator tensor is equal to zero, $s_r + 2s_\theta = 0$, and if yield condition $\sigma_r - \sigma_\theta = f_2(\theta)$ holds, one obtains $s_r = 2f_2(\theta)/3$, where s_r and s_θ are radial and circumferential components of the stress deviator tensor.

System of partial differential equations (1) for σ_r and υ will be written as follows:

$$\begin{aligned} &\frac{1}{K_1}\left(\frac{\partial\sigma_r}{\partial t} + \upsilon\frac{\partial\sigma_r}{\partial r}\right) + (1-\theta)\left(\frac{\partial\upsilon}{\partial r} + \frac{2\upsilon}{r}\right) = 0, \\ &\frac{\partial\sigma_r}{\partial r} + \frac{2f_2(\sigma_r)}{r} = -\frac{\rho_0}{1-\theta}\left(\frac{\partial\upsilon}{\partial t} + \upsilon\frac{\partial\upsilon}{\partial r}\right), \end{aligned} \tag{22}$$

where $1 - \theta = 1 - f_1^{-1}(\sigma_r)$, $\sigma_r = f_1(\theta) \equiv f_3(\theta) + \frac{2}{3}f_2(\theta)$, $K_1 = \frac{\partial f_1(\theta)}{\partial\theta}$.

On the boundary of the expanding cavity of radius $R_0 = V_0 t$, velocity V is assigned, outer surface of the spherical layer R_∞ is free from stresses, and the velocity and stresses in the medium at the initial time are equal to zero:

$$\upsilon(R_0, t) = V, \sigma_r(R_\infty, t) = 0, \upsilon(r, 0) = \sigma_r(r, 0) = 0. \tag{23}$$

3.2.2 Formulation of a boundary-value problem for a system of first-order ordinary differential equations

A self-similar solution of the system for variable $\xi = r/ct$ will be considered, and dimensionless variables $U = \upsilon/c$, $S_r = \frac{\sigma_r}{\rho_0 c^2}$ will be introduced together with the following notations: $\tilde{f}_{1,2} = \frac{f_{1,2}}{\rho_0 c^2}$, $\tilde{K}_1 = \frac{\partial \tilde{f}_1}{\partial \theta}$. The partial derivatives in time and space are defined similarly to Section 3.2.1.

As a result of the substitution, the system of partial differential Eq. (22) is transformed into a system of ordinary differential equations:

$$U' + 2\frac{U}{\xi} = \frac{(\xi - U)}{(1-\theta)\,\tilde{K}_1} S_r',$$
$$S_r' + 2\frac{\tilde{f}_2}{\xi} = \frac{(\xi - U)}{1-\theta} U', \tag{24}$$

where $1 - \theta = 1 - \tilde{f}_1^{-1}(S_r)$, and prime denotes differentiation with respect to ξ

Boundary conditions (23) for equation system (24) are defined depending on the relation of velocities c and c_e, and value $\alpha = c/c_e$. For $0 < \alpha < 1$, the boundary conditions are defined by an elastic solution (Appendix A). For $\alpha \geq 1$, Hugoniot's jump conditions (5) are used, from which it follows that $\theta = \upsilon/c$, $\upsilon/c = \sigma_r/\rho_0 c^2$ or, in dimensionless variables, $U = S_r = \theta$.

Finally, the boundary-value problem for a system of two first-order ordinary differential equations, written in a normal form, is as follows:

$$U' = \frac{2\left(U\tilde{K}_1 + \tilde{f}_2\Phi\right)}{\xi\left(\Phi^2 - \tilde{K}_1\right)}, \quad S_r' = \frac{2\tilde{K}_1\left(\tilde{f}_2 + U\Phi\right)}{\xi\left(\Phi^2 - \tilde{K}_1\right)}, \ \varepsilon < \xi < 1,$$
$$U(\xi = \varepsilon) = \varepsilon,$$
$$U(\xi = 1) = \begin{cases} U^e, \ \alpha < 1 \\ \theta_1, \ \alpha \geq 1 \end{cases}, S_r(\xi = 1) = \begin{cases} S_r^e, \ \alpha < 1 \\ \theta_1, \ \alpha \geq 1 \end{cases}, \tag{25}$$

where $\Phi = (\xi - U)/(1 - \theta)$, and θ_1 is the solution of equation $\tilde{f}_1(\theta) = \theta$.

Equation system (25) includes the unknown parameter c, that is the velocity of propagation of the plastic-elastic interface for $c < c_e$ or the plastic-unperturbed interface velocity for $c > c_e$. The unknown velocity c is determined iteratively, as long as boundary condition $|U(\xi = \varepsilon) - \varepsilon| < \delta$ is satisfied to an assigned accuracy δ. At each iteration step, the fourth-order-accurate Runge–Kutta numerical method is used for self-similar variable ξ changing from elastic–plastic interface (ξ =1) to cavity boundary ($\xi = \varepsilon$).

4 Analyzing the accuracy of the approximate solution

4.1 Parametric analysis of the cavity problem solution with Mohr–Coulomb yield criterion

The problem of spherical cavity expanding at a constant velocity from a zero radius in an infinite nonlinearly compressible medium is considered. Compressibility of the medium is characterized by linear relation (8) between shock wave velocity and mass velocity of the particles of the medium. Resistance of the medium to shear is assigned by Mohr–Coulomb's linear relation. Cavity expansion velocity, internal friction coefficient and parameter of dynamic compression strength are varied.

4.1.1 Verification of the numerical solution method

The technique for numerical solution of the boundary-value problem (25) for a system of two ordinary differential equations of the first order will be verified as compared to the numerical results obtained in [5,19,55].

In [55], the problem of equilibrium of a spherical cavity subjected to internal pressure in a linearly compressible medium was considered, the shear properties of which depend on the pressure:

$$f_3(\theta) \equiv K\theta, \quad f_2(\theta) \equiv \tau + kp,$$

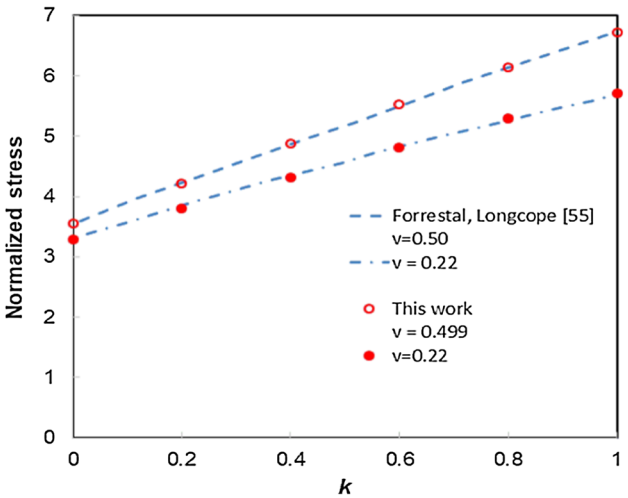

Fig. 5 Normalized radial stress at the cavity wall σ_C/Y via pressure-dependent shear stress coefficient k

$$f_1(\theta) \equiv K\theta + \frac{2}{3}(\tau + kp)$$

where K is bulk modulus of compression, $E = 3K(1-2\nu)$ is Young's modulus, ν is Poison's ratio, $\tau = \frac{3-k}{3}Y$, and Y is uniaxial compressive strength.

This formulation of the problem was realized within the framework of the system (25) at cavity expansion rate close to 0 and parameters: E = 221 GPa, Y = 1.93 GPa, $\nu = 0.22$ and 0.5 [55]. The results of numerical calculations, namely the dependence of the radial stresses at cavity boundary on the coefficient k, are shown in Fig. 5 by markers while the results of [55] are shown by dashed and dash-dotted lines. A complete agreement of the results is observed.

Examples of solving dynamic problems for a compressible material with account for strain hardening are given in [5] and [19]. However, the plasticity model employed does not make use of the normality principle to deduce plastic strain rate components. The plastic potential is here replaced by an equation of state, so strain hardening cannot be implemented in a similar analysis. Some correspondence can be obtained by assuming elastic deformations to be small in comparison with plastic ones. Let us assume

$$f_3(\theta) \equiv K\theta, \quad f_2(\theta) \equiv \tau\left(\frac{E\theta}{\tau}\right)^n,$$
$$f_1(\theta) \equiv K\theta + \frac{2}{3}\tau\left(\frac{E\theta}{\tau}\right)^n$$

where n is hardening modulus.

The calculations were carried out at: E=500 MPa, τ = 1.5 and 50 MPa, n=0.1 and 0.3, ν =0, 0.3 and 0.499. For the chosen values, we have $\sqrt{E}/\rho_0$ =500 m/s.

Figure 6 a presents the normalized stresses σ_C/τ at cavity boundary expanding with a velocity $m=V/\sqrt{E}/\rho_0$, obtained numerically in [19] (solid and dashed lines) and in the present work (light points) with varying the index n=0.1 and 0.3 at ν =0.3 and τ/E =0.003; the dash-dotted line in Fig. 5 corresponds to the results of [5] for an incompressible ideal-plastic Mises material at τ/E =0.01, the dark dots show the results of this work obtained at the values ν = 0.499 and n = 0.

Figure 6, b shows the results of similar calculations [19] with varying Poisson's ratio ν =0 and 0.499 at τ/E =0.003.

With the exception of the region of cavity expansion at low velocities, elastic deformations are comparable with plastic ones. A fairly good agreement between the calculation results can be noted in Fig. 5 that testifies to the efficiency of the implemented numerical technique for solving dynamic problems with shock waves.

Subsequently, the nonlinear law of bulk compressibility determined by the shock adiabat experimentally obtained for the granular medium was used in calculations.

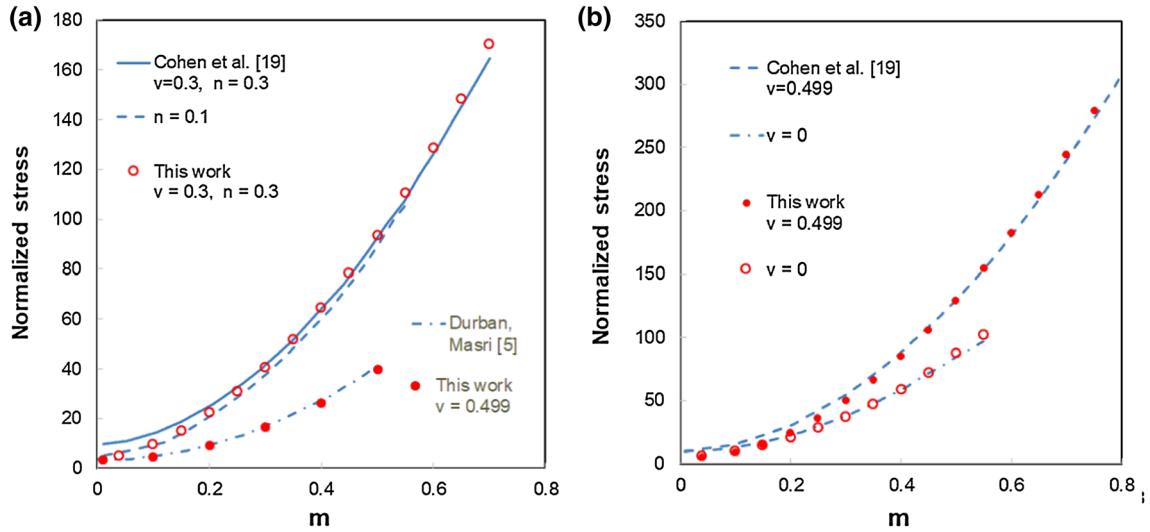

Fig. 6 Normalized stress at the cavity wall σ_C/τ expanding at dimensionless velocity $m = V/\sqrt{E/\rho_0}$

Table 2 Parameters of the Soil1 and Soil2

№	ρ_0, kg/m^3	K, MPa	G, MPa	c_e, m/s	C_0, m/s	s	σ_0, MPa	k	μ
1	1730	220	115	465	460	2.3	0.042	1.0	0.6
2	2080	4570	1147	1713	1700	3.4	0.021	0.5	0.375

4.1.2 Formation of a plastic shock wave

As it was noticed in Sect. 3.2, the solution of the problem in the plastic region is continuous at the transition to the elastic region for $c < c_e$ and there is no elastic region for $c > c_e$, but only unperturbed space which the solution is discontinuous at the plastic-unperturbed space interface. Further, two choices of the parameters of the equation of state of a medium with known stress-volumetric strain (shock adiabat) relations and Mohr–Coulomb's yield criterion are considered as an illustration, which are listed in Table 2. In what follows, media Soil1 and Soil2 will be considered.

The curves in Fig. 7 correspond to the results of the solution of the boundary-value problem for a system of ODE (Section 3.2, Eqs. (25)), using the fourth-order-accurate Runge–Kutta method. In what follows, this solution will be called "exact solution."

It is found that a shock wave is formed at cavity expansion velocities $V = V_s$ (marked in dotted lines), $V_s = 182$ m/s and 550 m/s for Soil1 and Soil2, respectively. In the vicinity of these values, the solution curves have second-order tangency.

In Fig. 8, velocity is represented on a logarithmic scale, and the dashed line corresponds to the value of the dimensionless cavity expansion velocity $M_s \equiv V_s/C_0$, at which a single plastic shock wave is formed ($M_s = 0.395$ and $M_s = 0.340$ for the Soil1 and Soil2, respectively).

The exact solution in Fig. 8 demonstrates the limitation of parameter ε when the cavity expansion velocity tends to infinity ($\varepsilon < 0.758$ and $\varepsilon < 0.663$ for Soil1 and Soil2, respectively) and to zero ($\varepsilon > 0.066$ and $\varepsilon > 0.023$ again for Soil1 and Soil2, respectively). The approximate solutions according to formulas (12) are limited from above ($\varepsilon < 1/\sqrt[3]{s}$). The dimensional stress value on the cavity wall also remains limited at velocities close to zero: for Soil1, the stress does not exceed 2.3 MPa, and for the Soil2 it does not exceed 1.13 MPa. The value of ε, obtained using formula (13a), is close enough to the exact solution, except for the region with $M < 0.1$, the solution according to linearized formula (13b) tends to the exact solution only at $M > 0.4$.

The evaluation of the minimal stress on the cavity wall, required for its propagation, in a compressed linearly elastic medium with pressure-dependent shear strength was obtained earlier in [55].

The linearized *rigid–plastic* solution (13b) in Fig. 9 appears to be closer to the exact solution for $M > 0.4$, than the *rigid–plastic* solution according to Cardano's formula (13a).

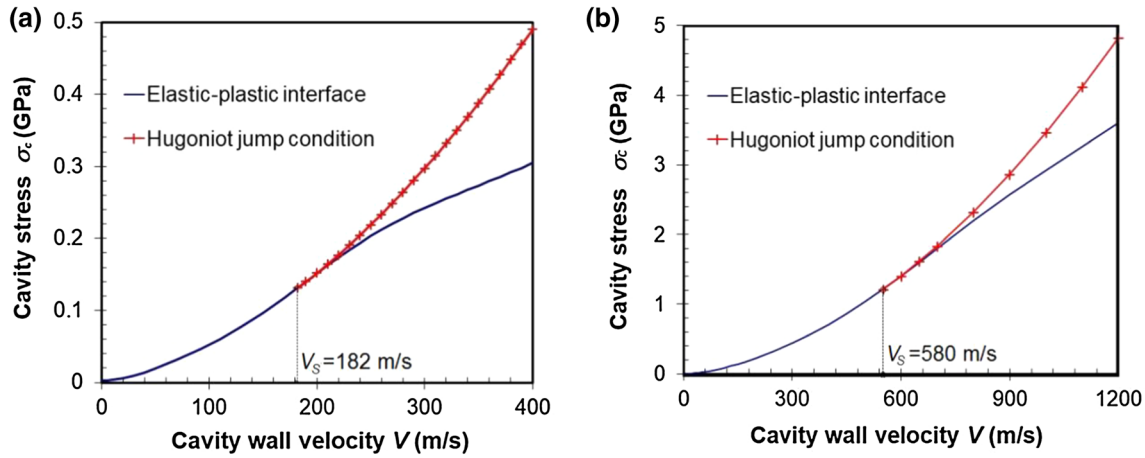

Fig. 7 Stress at the boundary of a cavity expanding at velocity V for the Soil1 (a) and Soil2 (b): elastic–plastic solution for $V \leq V_s$ (solid line) and the solution indicating the formation of a single plastic shock wave propagating through the unperturbed medium (the crossed solid line) for $V > V_s$

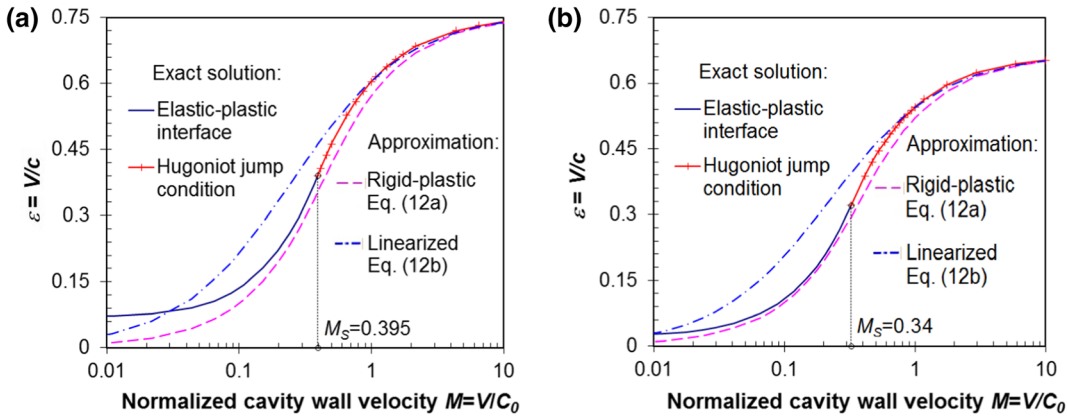

Fig. 8 Dimensionless parameter ε as a function of cavity expansion velocity in relation to elastic wave velocity for the Soil1 (a) and Soil2 (b): exact generalized solution including elastic–plastic interface (the solid blue line) at $M \leq M_s$ and formation of a plastic shock wave (the solid red line with a cross) at $M > M_s$, approximated *rigid–plastic* solution (12a) (the dotted line) and *linearized rigid–plastic* solution (12b) (the dot-dash line)

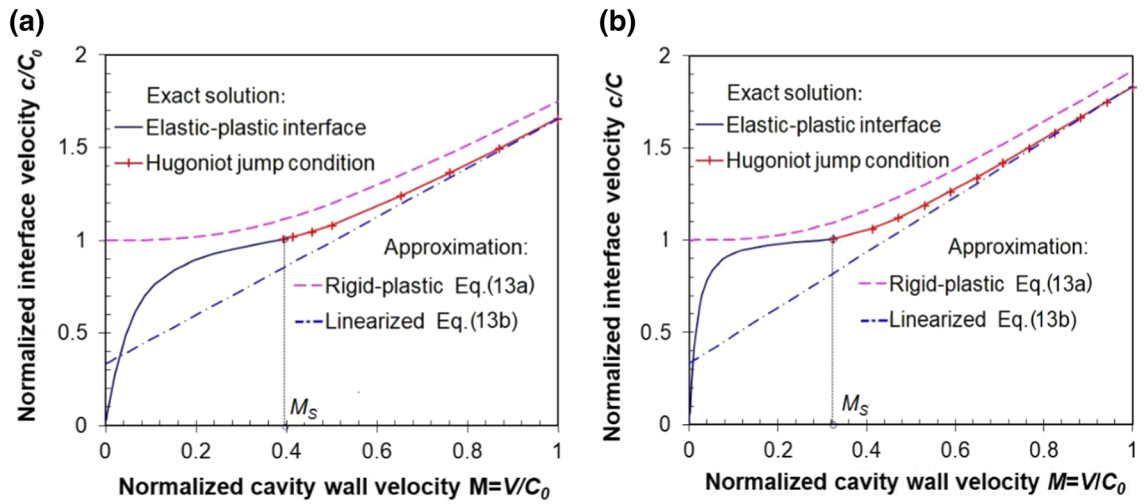

Fig. 9 Normalized propagation velocities of the elastic–plastic interface as a function of cavity expansion velocity for the Soil1 (a) and Soil2 (b): (the definition of the curves is the same as in Fig. 8)

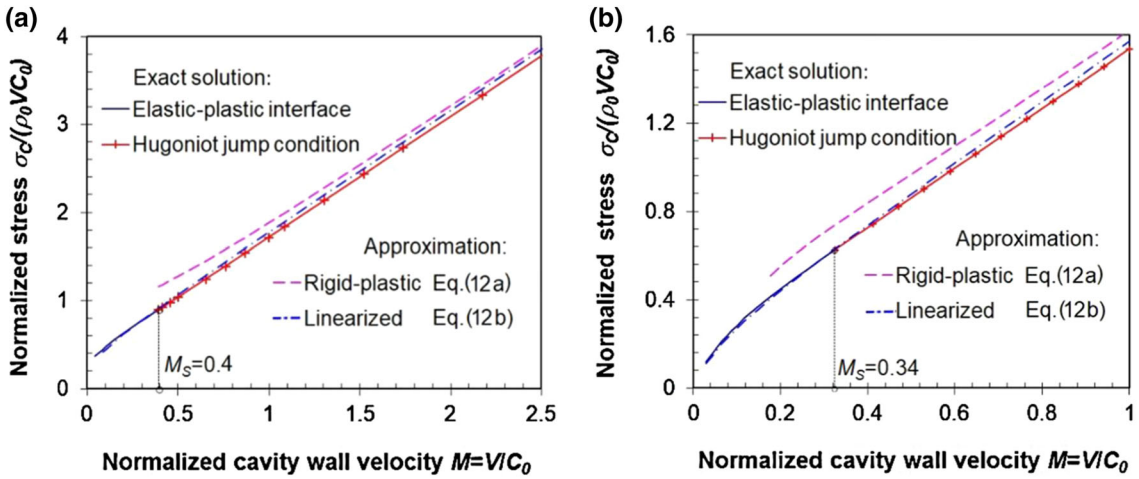

Fig. 10 Dimensionless relations between stress on the cavity wall expanding at velocity V for the Soil1 (**a**) and Soil2 (**b**): (the definition of the curves is the same as in Fig. 8)

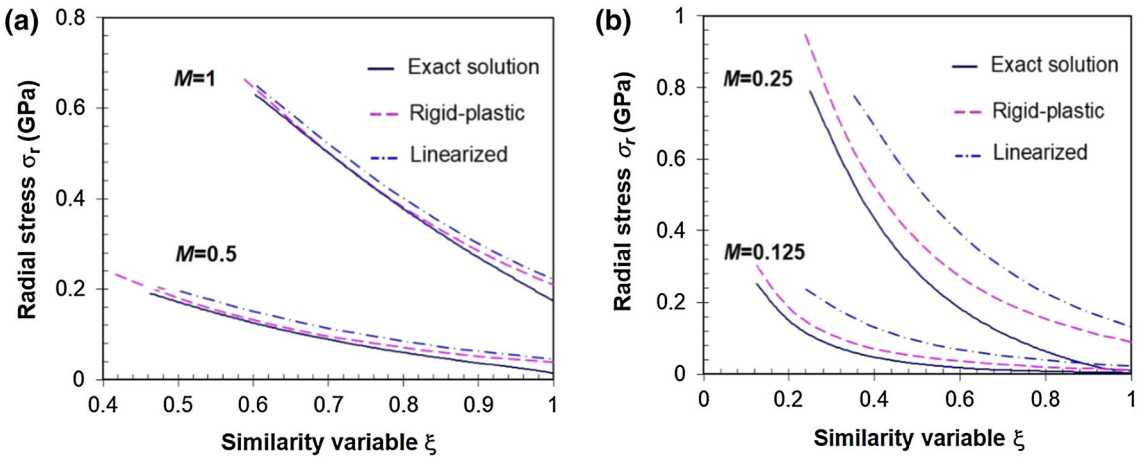

Fig. 11 Stress distribution in the medium as a function of similarity variable ξ at the dimensionless cavity expansion for velocities M =0.5 and M =1.0 for the Soil1 (**a**), M =0.125 and M =0.250 for the Soil2 (**b**): the solid, dotted and dot-dash lines correspond to the exact generalized solution, the *rigid–plastic* and *linearized* rigid–plastic solutions, respectively

It has to be noticed that solving the problem without accounting for the formation of a plastic shock wave results in the limitation of the elastic–plastic interface at high cavity expansion velocities (the solid line in Fig. 9), which agrees with the results earlier obtained in [16]. The continuation of the solution, concentrating on the single plastic shock wave (the solid line with a cross in Fig. 8), is closer to the physical picture of wave propagation.

The approximate solutions in Fig. 10 were obtained using formulas (12a), (17a) and (12b), (17a), respectively. The approximate linearized solution agrees well with the exact solution in a complete formulation over a fairly wide range of cavity expansion velocities up to M =0.1. Like the exact solution, the dimensionless linearized solution has a nonlinear character at $M < 0.4$, and at $M > 0.4$ can be represented by a linear relation.

The good agreement between the approximate linearized and the exact solutions can be explained if stress distributions in the medium as a function of the dimensionless coordinate is considered.

It is evident in Fig. 11 that the computations of stress using Eq. (12a) for determining $\varepsilon$and Eq. (13a) for determining shock wave velocity generally give closer results than those obtained using the linearized formulas (12b) and (13b), respectively. However, maximal stress values in the vicinity of the cavity, obtained using formulas (12b), (17b) (the dot-dash line in Fig. 10), tend to be closer to the exact value.

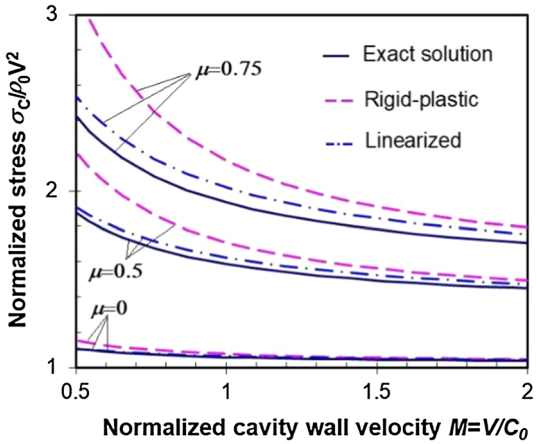

Fig. 12 Normalized stresses at the cavity wall as a function of dimensionless expansion velocity, obtained for the values: μ =0; μ =0.5; μ =0.75. (definitions are the same as in Figs. 10, 11)

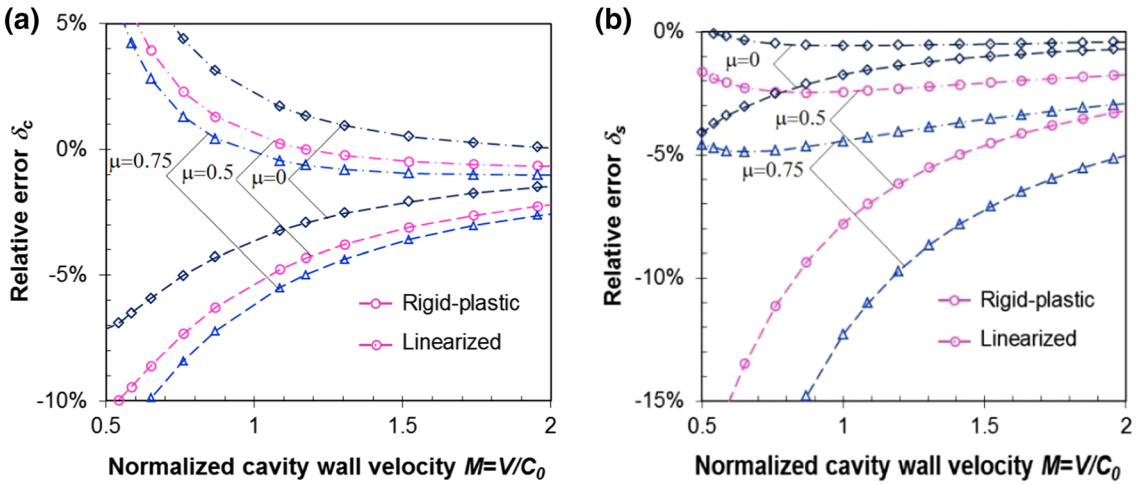

Fig. 13 Relative error in determining the shock wave front velocity (a) and the stress at the cavity wall (b) for μ =0, μ =0.5 and μ =0.75

The formal continuation of solution (13) into the region with $M < 0.4$ for the Soil2 leads to an error of 13% and 16% in defining the stress at the cavity boundary. Errors in determining stresses using formulas (12b), (17b) substantially decrease with an increasing cavity expansion velocity.

4.1.3 Evaluation of stress at the cavity wall

In what follows, the normalized stresses obtained in the framework of the problem of spherical cavity expansion, by varying the internal friction coefficient, are compared; the remaining parameters correspond to the material with Soil1.

It follows from Fig. 12 that the difference between the stresses obtained exactly and approximately decreases with the cavity expansion velocity. This corroborates the earlier conclusion that linear relation (13b) of shock wave velocity as a function of cavity expansion velocity is more accurate in determining normal stress at the cavity wall than the exact solution using Cardano's formulas (13a).

This is connected with a summation of errors of opposite sign. The difference between the approximate and exact solutions increases with μ, the character of the curves remaining the same. The minimal error of the approximate solutions is observed for a value of the internal friction coefficient close to 0.

Figure 13a depicts relative errors in determining the plastic shock wave velocity for various values of internal friction coefficient $\delta_c = \left(c - c_{a,b}\right)/c \cdot 100\%$, where c is the exact solution, and c_a and c_b are determined from formulas (13a) and (13b). The relative errors for the stress at the cavity wall depicted in Figs. 15b are determined

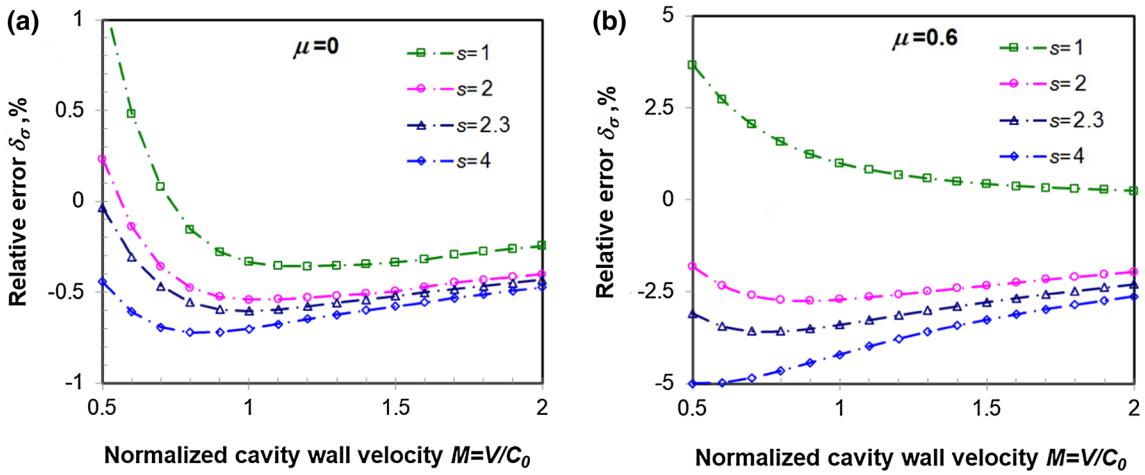

Fig. 14 Relative errors in determining the cavity wall stress for various values of slope s of the soil for $\mu = 0$ (a) and $\mu = 0.6$ (b) as a function of relative cavity expansion velocity $M = V/C_0$

in a similar way. The relative errors for approximate linearized formulas (17b), (12b) are significantly lower than those using Cardano's formulas (12a). The errors are also observed to decrease with an increasing cavity expansion velocity. Thus, velocities and stresses at the wall of a spherical cavity, expanding at a constant velocity from zero radius in a soil medium with a known shock adiabat, are determined using formulas (13b) and (17), (12b) with an error less than 5% at relative cavity expansion velocities $M = V/C_0 > 0.4$ and when the variation of the μ is in the range [0; 0.75].

The error in Fig. 14 was determined in a standard way: $\delta_\sigma = (\sigma_C - \sigma_b)/\sigma_C \cdot 100\%$, where σ_C is the exact solution, and σ_b is determined using formulas (17b), (12b) for μ =0 and formulas (3), (12b) for μ =0.6. It can be seen that the errors in determining the stress at the wall of the spherical cavity, expanding at a constant velocity in a soft medium, using linearized formula (12b) and formula (17b) do not exceed 5% at relative cavity expansion velocities $M = V/C_0 > 0.5$ and compression strength parameter s changing in a fairly wide range [1; 4] for admissible values of the internal friction coefficient.

Determining the plastic shock wave velocity using formula (13b) and the stress at the cavity wall using Eqs. (12b), (17b) can formally be extended onto the range $M < 0.5$.

It is evident from Fig. 15 that at relative cavity expansion velocity $M < 0.5$ the error in determining the shock wave velocity increases up to 50%. For stresses calculated at the cavity wall, the errors do not exceed 5% over the entire velocity range, and only, the errors increase up to 10%. The obtained estimations show that equations (17) and the linearized Eqs. (12b), (13b) can be further used for approximating stresses at the cavity wall when analyzing problems of penetration into soil media for relative cavity expansion velocities $M > 0.1$.

5 Determining the force resisting penetration of a rigid sphere into sand

5.1 Parameters of the soft soil model

The model of a soft soil includes a high-pressure equation of state, an elasticity moduli K and G of the initial part of the deformation curve, as well as a plasticity condition. Representing the shock adiabat defined by the Rankine–Hugoniot equations in the form of linear relation [52] (8) makes it possible to correlate stress σ_r and volumetric strain θ in conditions of uniaxial deformation:

$$f_1(\theta) \equiv \rho_0 C_0^2 \theta (1 - s\theta)^{-2}. \tag{26}$$

Resistance of the medium to shear is defined by a nonlinear relation between yield stress and pressure:

$$f_2(p) \equiv \sigma_0 + kp/(1 + kp/\Delta\sigma),\ \Delta\sigma = \sigma_1 - \sigma_0. \tag{27}$$

Coefficients σ_0, σ_1 and k in (27) characterize cohesion, maximal value of yield stress and tangent of the internal friction angle of the soil.

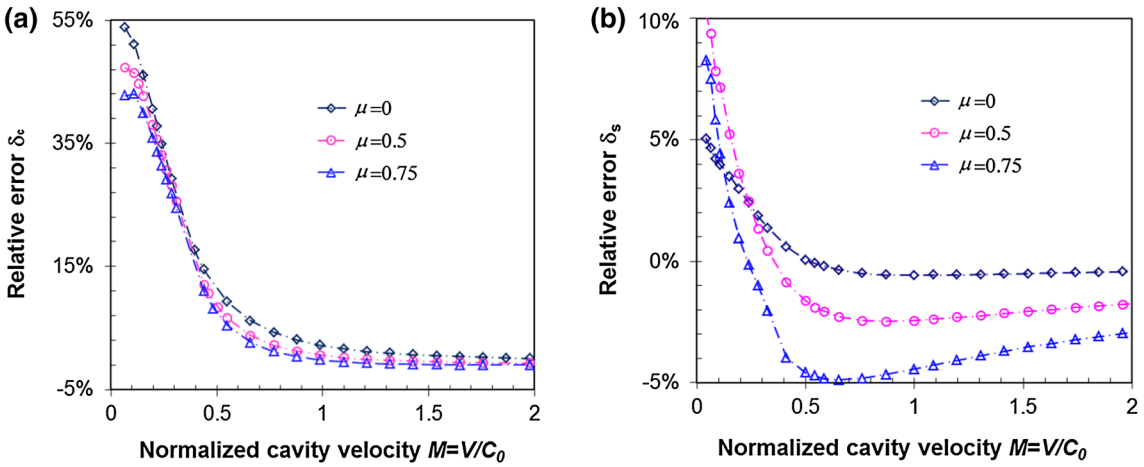

Fig. 15 Error in determining shock wave front velocity (**a**) and cavity wall stress (**b**) using the linearized rigid–plastic solution for the values of μ =0, μ =0.5 and μ =0.75

Table 3 Sand model parameters for different water saturation

No	w, %	ρ_0, kg/m^3	C_0, m/s	s	a, m/s	b	σ_0, MPa	k	σ_1, MPa
1	0	1730	460	2.3	340	2.6	0.1	1.2	275
2	20	2080	1700	3.4	1620	3.6	0.1	0.5	50

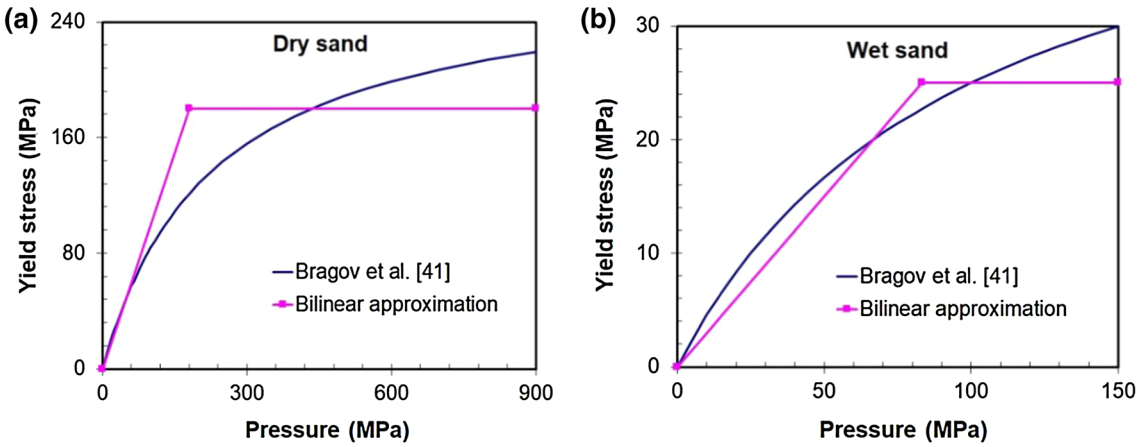

Fig. 16 Bilinear relations between yield stress and pressure for dry (a) and wet sands (b) and Mohr–Coulomb Tresca's bilinear approximation

For the "pressure-volumetric strain" relation the following function of the form (26) is used:

$$p = f_3(\theta) \equiv \rho_0 a^2 \theta \, (1 - b\theta)^{-2}, \tag{28}$$

where the unknown parameters a and b are found by using the least squares method.

We defined the shock adiabats parameters C_0 and s for dry and wet sand based on results of plane-wave shock experiments [49,51,56]. These parameters were close to those obtained earlier in the inverse impact experiment technique by using a measure bar with flat end [44]. The following Table 3 lists the parameter values for the dry and water-saturated sands.

Figure 16 presents curves of nonlinear yield criterion (27) as approximated by the bilinear relations of Mohr–Coulomb's with Tresca's limit yield criterion

$$f_2 \equiv \begin{cases} \tau + kp = \tau_0 + \mu\sigma_r, & 0 < \sigma_r \le \sigma_{\mathrm{M}}, \\ \tau_M, \quad \sigma_r > \sigma_M. \end{cases} \tag{29}$$

Table 4 Parameters of yield criterion (29) for dry and wet sand

$\mathcal{N}_o$	τ, MPa	k	μ	τ_M, MPa	σ_M, MPa
1	0.042	1.0	0.6	180	300
2	0.021	0.3	0.25	25	1000

Table 5 Limits of the chosen ranges in equations (19) and (20)

$\mathcal{N}_o$	V_0, m/s	V_M, m/s	ε_0	ε_M	V, m/s	ξ_M	S_M
1	296	528	0.544	0.607	400	0.795	0.298
2	150	380	0.19	0.305	250	0.58	0.053

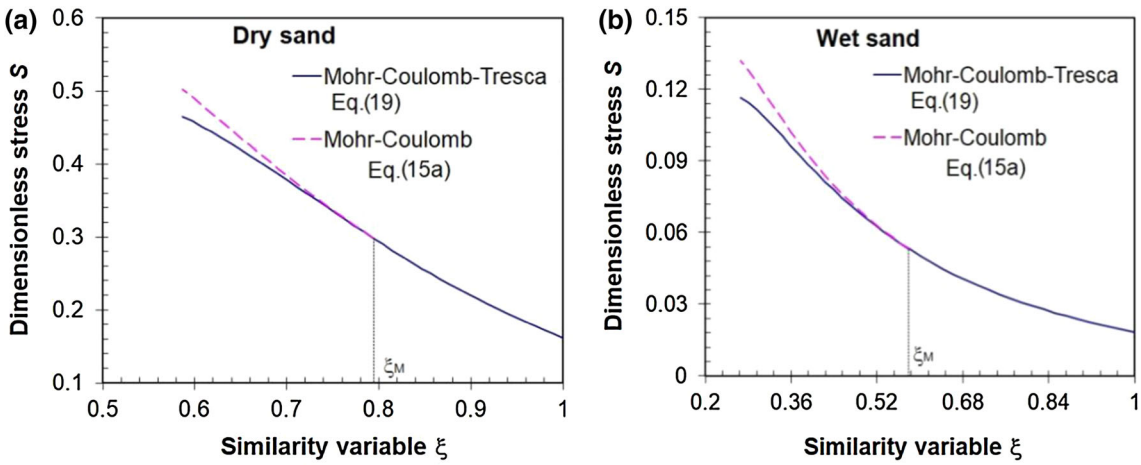

Fig. 17 Distribution of dimensionless stresses as a function of self-similar coordinate in dry (**a**) and wet (**b**) sand for Mohr–Coulomb Tresca's yield criterion (the solid line) and Mohr–Coulomb's criterion (the dotted line)

Equation (29) is approximate. Its error is determined directly in the calculations of the resistance force to the penetration of the sphere into the sand. The parameters of yield criterion (29) for dry and wet sand are presented in Table 4

The parameters of the elastic portion of the deformation diagram and the shock adiabat of dry and wet sands are those previously presented in Table 2.

5.2 Analytical solution of the spherical cavity problem with Mohr–Coulomb Tresca's limit yield criterion

In Fig. 16, the cavity expansion velocities are 400 and 250 m/s for dry (a) and wet (b) sands, respectively. The values of parameters V_0 and V_M, determined using formulas (18), and the values of other parameters are summarized in Table 5:

In Table 5, the first and second lines correspond to dry and wet sand, respectively.

In Fig. 18, the markers represent normalized cavity wall stresses as a function of normalized expansion velocities under high pressures. Using Mohr–Coulomb's yield criterion (a), the stresses were found according to formula (3) for $M > 0.4$; the parameters of the equation of state are listed in Table 2. With Mohr–Coulomb Tresca's yield criterion (b), formula (17b) was used with $\tau_0 = \tau_M$, $V > V_M$; the parameters of the equation of state are listed in Table 3.

It can be seen that when using Mohr–Coulomb's yield criterion, the relation between stresses acting on the cavity wall and the velocity is $\sigma_r / \rho_0 = a_2 V^2 + b_1 V$ (see also [57]), whereas when Tresca's yield criterion is used for $\tau_0 = \tau_M$, $V > V_M$, the relation is $\sigma_r / \rho_0 = a_2 V^2 + a_0$; besides, $a_0 \approx 0$ for the wet soil.

It can be seen in Fig. 19 that the cavity wall stresses in the medium with Mohr–Coulomb Tresca's yield criterion can, accurately enough for engineering purposes, be determined without using Eqs. (6), (7), by employing interpolation over the cavity expansion velocity range $V_0 \le V \le V_M$.

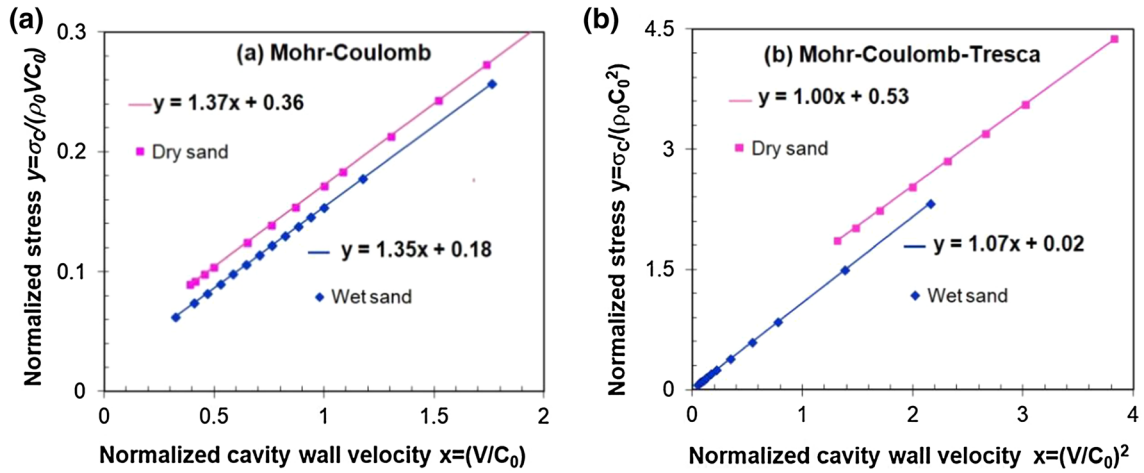

Fig. 18 Normalized cavity wall stresses as a function of normalized cavity expansion velocities when using Mohr–Coulomb's (**a**) and Mohr–Coulomb Tresca's limit (**b**) yield criterions in dry and wet sand (squares and diamonds, respectively) and linear approximations using the least squares method (solid lines)

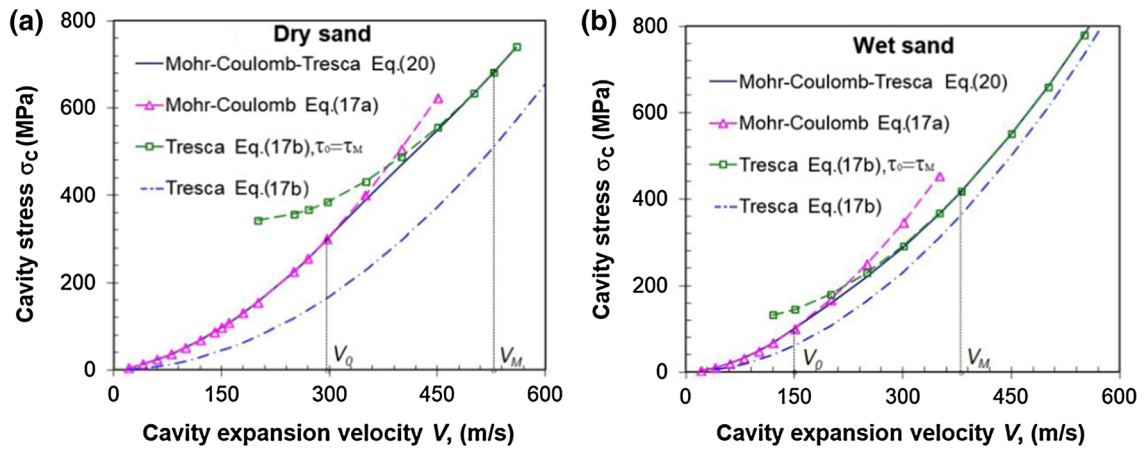

Fig. 19 Approximation of the cavity wall stress as a function of cavity expansion velocity in dry (a) and wet (b) sands: the solid line, the dotted line with triangles, the dash-dot lines and the dashed line with squares correspond to the results obtained using Eqs. (20), (17a), (17b) and (17b) for $\tau_0 = \tau_M$

5.3 Comparing the numerical and experimental results

Next, a comparison is made of the maximum resistance to the penetration of a projectile with a hemispherical head into sandy soil obtained in physical reversed experiments [44] with calculation data based on the SCE approximation.

As noted above, in a reversed experiment, a container with soil interacts with the initial velocity U_0 with a fixed measuring rod-striker. A scheme of the interaction of a stationary projectile with a hemispherical head of radius R with an incoming soil flow is shown in Fig. 20.

In Fig. 20 introduced a fixed coordinate system r0z with the beginning in the center of the midsection of the hemispherical part of the striker. Axis $0z$ is directed along the symmetry axis of the projectile, $h = -R + U_0 t$ is the current penetration depth ($-R \le h \le 0$), t is current penetration time; angle φ is counted from the apex of the sphere in the direction of the free surface corresponding to penetration depth $z = -R\cos\phi$.

The maximum force of contact interaction is achieved when a projectile with a hemispherical head penetrates to a depth not exceeding R. The dimensions of the soil container in the inverted experiment were chosen in such a way [41] that stress waves reflected from the walls and bottom of the container did not distort the stress state on the contact surface. In this case, the decrease in the average container speed at least in the time interval $0 < t < R/U_0$ is slightly. Therefore, the problem in the inverse formulation (see Fig. 20) can be

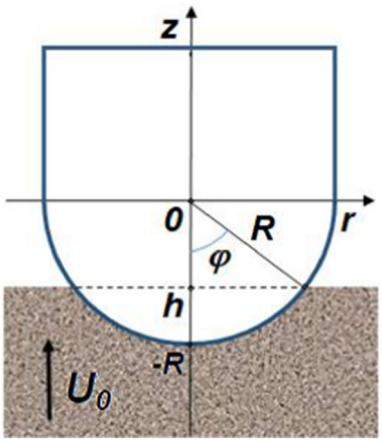

Fig. 20 Scheme of a projectile with a hemispherical head into sandy soil in a reversed formulation

considered with good accuracy equivalent to the problem of penetration of the impactor into the ground at a constant speed.

The force acting on a spherical head projectile penetrating into soil at constant velocity U_0, equal to impact velocity, is determined by integrating stresses over the contact surface and is related with the form and penetration velocity of the projectile as

$$F = -2\pi \int_{-R}^{h} \left(\sigma_n z + \sigma_\tau \sqrt{R^2 - z^2}\right) dz, \tag{30a}$$

where $\square = -R + U_0 t$ is the current penetration depth, $-R \leq \square \leq$, t is current penetration time, σ_n is normal stress, and σ_τ is tangential stress acting on the lateral surface of the spherical impactor.

Equation (30a) can be transformed as follows:

$$F = 2\pi R^2 \int_{0}^{\phi} (\sigma_n \cos\phi + \sigma_\tau \sin\phi) \sin\phi \, d\phi. \tag{30b}$$

According to the SCE approximation normal stress acting on the lateral surface of the projectile is identified with the radial stress acting at the surface of a spherical cavity expanding at a constant velocity in an infinite medium starting from a zero initial radius. As it was shown above, this stress can be represented in the form of a quadratic relation

$$\sigma_n/\rho_0 = a_2 U_n^2 + b_1 U_n, \tag{31}$$

where $U_n = U_0 \cos\phi$ is the normal component of the penetration velocity vector, and a_2, b_1 are constant coefficients depending on the physical-mechanical properties of the medium.

Tangent stresses on the surface of the body moving through the medium will be defined according to Coulomb's friction model

$$\sigma_\tau = k_f \sigma_n, \tag{32}$$

where k_f is a constant coefficient of surface friction.

After integrating Eq. (30), taking into account (31), (32), resistance to a spherical penetrator as a function of impact velocity will have the following form:

$$F = AU_0^2 + BU_0,\ A = a_2(A_1 + k_f A_2)\rho_0 S_0,\ B = b_1(B_1 + k_f B_2)\rho_0 S_0, \tag{33}$$

where $A_1 = (1 - \cos^4\phi)/2$, $A_2 = (\phi - 2\sin\phi\cos^3\phi + \sin\phi\cos\phi)/4$, $B_1 = 2(1 - \cos^3\phi)/3$, $B_2 = 2\sin^3\phi/3$, $S_0 = \pi R^2$ is the cross section area of the sphere. Substituting into (33) the values of ϕ, equal to

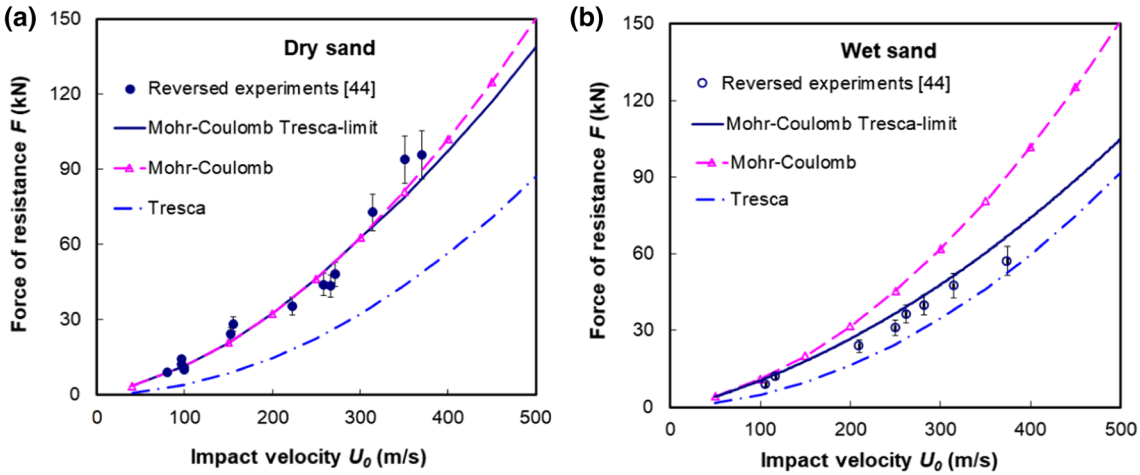

Fig. 21 Resistance force to penetration of a rigid spherical striker into dry (**a**) and wet (**b**) sand as a function of impact velocity: the reversed experiments [44] (the dark and light dots) and the approximation using the solution of the cavity expansion problem (the definition of the curves is the same as in Fig. 17)

a flow separation angle, $\phi*$, yields the maximum values of the force resisting penetration in the framework of SCE approximation, taking into account surface friction.

The flow separation angle was taken to be $\phi* = \pi/3$, the friction coefficient for dry sand was $k_f = 0.4$, and for wet sand $k_f = 0.2$. These values were assumed to be proportional to the internal friction coefficient, i.e., remained constant at $u < V_0$. At $u > V_M$, the values of the sliding friction coefficient were assumed to be equal to $k_f = 0$, over the interval $V_0 < u < V_M$ a linear interpolation was used.

Figure 21 demonstrates good agreement between the approximation results and the experimental data for both dry and water-saturated sand without introducing any correction factors. In the velocity range, for which the experimental data for dry sand were obtained (impact velocities up to 400 m/s), Mohr–Coulomb's yield criterion is true, whereas Tresca's limit comes to produce significant effects at impact velocities over 500 m/s.

The use of Mohr–Coulomb's with Tresca's limit yield criterion is more justified for wet sand. At low impact velocities (up to 200 m/s), internal friction plays an important role, whereas at higher velocities the limitation of the yield strength in the framework of Tresca's yield criterion manifests itself.

Indeed, high-speed penetrators are here considered, where resistance to shear of the soil medium can be neglected. Normal pressure on the surface moving at velocity U_0 will be expressed by equation (17b) without the first addend: $\sigma_r = \rho_0 U_0^2 \left(3/2 - \varepsilon - \varepsilon^4/2\right)/\left(1 - \varepsilon^3\right)$. The stress on the contact surface will be written as $\sigma_r = \frac{1}{2} C_D \rho_0 U_0^2$, where C_D is resistance coefficient. Then, assuming that $\varepsilon = 1/\sqrt[3]{s}$ (upper bound), the evaluation of coefficient C_D as a function of shock adiabat parameter s will be: $C_D = \left(3 - \left(2 + 1/s\right)/\sqrt[3]{s}\right)/\left(1 - 1/s\right)$. With s varying in the range $1 < s < 4$, the resistance coefficient changes in the range $2 < C_D < 2.11$, which is close enough to the results of [58], where the values of the coefficient of resistance to a flat-nosed penetrator, $C_D \approx 2$, were obtained.

6 Conclusions

1. We defined the parameters C_0 and s of shock adiabats described by the Rankine–Hugoniot equations for both dry and wet sand based on famous plane-wave experimental data. These data were close to those obtained earlier in the reversed impact experiment technique by using a measure bar with a flat end.
2. As applied to the problem of the penetration of rigid bodies into granular media, a self-similar analytical solution has been obtained for a one-dimensional problem of the expansion of a spherical cavity from a zero radius in an infinite soil medium. The solution was obtained under the assumption of elastic–plastic deformation of the soil with the Mohr–Coulomb Tresca's limit yield criterion.
3. It is shown numerically that when solving the problem of cavity expansion in the granular media, it is necessary to take into account the formation of a plastic shock wave propagating through the undisturbed portion of the medium.

4. The parametric analysis of the linearized rigid–plastic solution showed that it is a good approximation of the dependence of pressure at the boundary of the spherical cavity on the speed of its expansion as applied to a wide class of granular media.
5. On the basis of the proposed analytical solution, a method has been developed for calculating the resistance force of a spherical rigid body to penetrate into sand. The dependence of the maximum value of the resistance force to the introduction of a rigid sphere into dry and water-saturated sand, when the impact velocity varies in the range from 50 to 400 m/s, has been obtained.
6. Comparison of the results for determining penetration resistance forces obtained analytically, numerically and experimentally showed their qualitative and quantitative good correspondence to each other. In this regard, when solving problems of penetration into granular media, a simple analytical solution can be successfully applied.

Acknowledgements The work was carried out with the financial support of the Ministry of Science and Higher Education of the Russian Federation (task 0729-2020-0054).

Appendix A

The equation of motion in system (1) is written, neglecting the convective components of the time derivative of velocity:

$$\frac{\partial \sigma_r}{\partial r} + 2\frac{(\sigma_r - \sigma_\theta)}{r} = -\rho\left(\frac{\partial \upsilon}{\partial t}\right), \upsilon = \frac{\partial u}{\partial t}.$$

The radial and circumferential small strains in an elastic medium in conditions of spherical symmetry are defined in terms of displacements as $\varepsilon_r = \frac{\partial u}{\partial r}$, $\varepsilon_\theta = \frac{u}{r}$. The stress-strain relation is described by Hooke's law:$-\sigma_r = \lambda\left(\frac{\partial u}{\partial r} + 2\frac{u}{r}\right) + 2G\frac{\partial u}{\partial r} = (\lambda + 2G)\frac{\partial u}{\partial r} + 2\lambda\frac{u}{r}$, $\sigma_r - \sigma_\theta = 2G\left(\frac{u}{r} - \frac{\partial u}{\partial r}\right)$. As before, stresses in compression are assumed to be positive.

The dynamic equation of an elastic medium in terms of displacements, in the case of spherical symmetry, is transformed into the following form:

$$\frac{\partial^2 u}{\partial r^2} + \frac{2}{r}\frac{\partial u}{\partial r} - \frac{2u}{r^2} = \frac{1}{c_e^2}\frac{\partial^2 u}{\partial t^2}, \tag{A1}$$

where $c_e = \sqrt{(\lambda + 2G)/\rho_0} = \sqrt{(K + 4G/3)/\rho_0}$ is the velocity of propagation of the longitudinal wave front in an elastic medium.

Following [3], it is assumed that $\xi = \frac{r}{ct}$, $\tilde{u} = u/ct$ are, respectively, a dimensionless coordinate and a dimensionless displacement,$c$is the plastic wave front velocity (i.e., the velocity of the elastic–plastic interface), then the derivatives are transformed as follows, accounting for these changes of variables:

$$\frac{u}{r} = \frac{\tilde{u}}{\xi}, \frac{\partial u}{\partial r} = \tilde{u}', \frac{\partial^2 u}{\partial r^2} = \frac{1}{ct}\tilde{u}'', \frac{\partial^2 u}{\partial t^2} = \frac{c}{t}\xi^2\tilde{u}''$$

where primes denote differentiation with respect to ξ.

The conditions on the boundary of the elastic deformation region are then considered. On the boundary with the unperturbed region, the displacement is equal to zero. On the elastic–plastic interface $\xi = 1$ the condition of plastic yield $(\sigma_r - \sigma_\theta)\big|_{\xi=1} = f_2(\theta)$ holds, as well as Hooke's law:$\sigma_r - \sigma_\theta = 2G\left(\frac{u}{r} - \frac{\partial u}{\partial r}\right)$, whence, due to the continuity of the stress components, one has: $\left(\frac{u}{r} - \frac{\partial u}{\partial r}\right) = \frac{f_2(\theta)}{2G}$, $\theta = -\left(\frac{\partial u}{\partial r} + 2\frac{u}{r}\right)$. Transformation of the derivatives and substitution into equation (A1) and boundary conditions yield the following boundary-value problem for a second-order ordinary differential equation in terms of the dimensionless displacement:

$$\left(1 - \alpha^2\xi^2\right)\tilde{u}'' + \frac{2\tilde{u}'}{\xi} - \frac{2\tilde{u}}{\xi^2} = 0, \alpha = c/c_e, \tilde{u}\left(\xi = 1/\alpha\right) = 0$$

$$\left(\frac{\tilde{u}}{\xi}-\frac{\partial\tilde{u}}{\partial\xi}\right)\Big|_{\xi=1}=\frac{f_2(\theta)}{2G},\theta=-\left(\frac{\partial\tilde{u}}{\partial\xi}+2\frac{\tilde{u}}{\xi}\right)\Big|_{\xi=1}. \tag{A2}$$

To find a general solution to the differential equation, several transformations are done. Substituting $w=\alpha\xi$, one obtains the following equation:

$$\left(1-w^2\right)\frac{d^2\tilde{u}}{dw^2}+\frac{2}{w}\frac{d\tilde{u}}{dw}-\frac{2\tilde{u}}{w^2}=0.$$

Substitutions $\tilde{u}=w\vartheta$, $Y=d\vartheta/dw$ yield a first-order equation for $Y(w)$: $w\left(1-w^2\right)Y'+2\left(2-w^2\right)Y=0$ or $\frac{dY}{Y}=-\frac{2\left(2-w^2\right)}{w\left(1-w^2\right)}dw$, a general solution for which is function $Y(w)=\frac{A}{w^2}-\frac{A}{w^4}$ depending on an arbitrary constant A. Then the series of transformations: $\frac{d\vartheta}{dw}=\frac{A}{w^2}-\frac{A}{w^4}$, $\vartheta(w)=\frac{A}{3w^3}-\frac{A}{w}+B$, $\tilde{u}=z\vartheta$: $\tilde{u}=\frac{A}{3w^2}-A+Bw$, result in the following expression for the dimensionless displacement: $\tilde{u}=A\left(1/3\alpha^2\xi^2-1\right)+B\alpha\xi$, where B is another integration constant.

To define constants A, B, the boundary conditions in problem (A2) are used. From the first boundary condition, it follows that $B=2A/3$, thus,

$$\tilde{u}=A\left(\frac{1}{3\alpha^2\xi^2}+\frac{2}{3}\alpha\xi-1\right)=A\frac{(1-\alpha\xi)^2(1+2\alpha\xi)}{3\alpha^2\xi^2}. \tag{A3}$$

Now by an expression for determining the dimensionless velocity

$$U=\tilde{u}-\xi\frac{d\tilde{u}}{d\xi},U(\xi)=A\left(\frac{1-\alpha^2\xi^2}{\alpha^2\xi^2}\right), \tag{A4}$$

the radial component of the stress tensor and the volumetric strain will be derived:

$$\sigma_r(\xi)=2A\frac{(1-\alpha\xi)}{\alpha^2\xi^3}\left(K\alpha^2\xi^2+\frac{2G}{3}(1+\alpha\xi)\right) \tag{A5}$$

$$\theta=-\left(\frac{\partial\tilde{u}}{\partial\xi}+2\frac{\tilde{u}}{\xi}\right)=2A\left(\frac{1-\alpha\xi}{\xi}\right). \tag{A6}$$

Employing now equality (A6), equations for both dimensionless velocity (A4) and stress (A5) can be transformed into the following form:

$$\begin{aligned}U(\xi)&=\left(\frac{1+\alpha\xi}{2\alpha^2\xi}\right)\theta(\xi),\\ \sigma_r(\xi)&=\left(K+\frac{2G}{3}\frac{(1+\alpha\xi)}{\alpha^2\xi^2}\right)\theta(\xi).\end{aligned} \tag{A7}$$

To define the integration constant A, the second boundary condition of the boundary-value problem (A2) is considered. Strain difference for $\xi=1$ is defined as $\left(\tilde{u}/\xi-\partial\tilde{u}/\partial\xi\right)\big|_{\xi=1}=A\left(\alpha^{-2}-1\right)$. Thus, constant A is determined by solving the equation $2GA\left(\left(1-\alpha^2\right)/\alpha^2\right)=f_2(2A(1-\alpha))$.

This problem was solved earlier in [3], using Tresca's yield condition. Consider Mohr–Coulomb Tresca's plasticity condition; in this case, function f_2 becomes:

$$f_2\equiv\begin{cases}\tau+kK\theta, & 0<\theta\le\theta_{\mathrm{M}},\\ \tau_M, & \theta\ge\theta_M\end{cases},\theta_M=\frac{\tau_M-\tau}{kK}.$$

So, for $\xi=1$ one has:

$$\theta=\begin{cases}\tau/(G(\alpha)-kK), & G(\alpha)>G^*,\\ \tau_M/G(\alpha), & G(\alpha)\le G^*,\end{cases} \tag{A8}$$

where: $G(\alpha)=(1+\alpha)G/\alpha^2$, $G^*=\tau_MkK/(\tau_M-\tau)=\tau_M/\theta_M$.

Expressions (A7), (A8) for $\xi=1$ will define the boundary conditions for the problem from Section 3.2. as a function of the value of α:

$$U^e = U\,(\xi = 1) = \frac{(1+\alpha)}{2\alpha^2}\theta,$$
$$S_r^e = S_r\,(\xi = 1) = \left(\tilde{K} + 2/3\tilde{G}\right)\theta, \tag{A9}$$

where θ is defined by expression (A6), $\tilde{K} = K/r_0c^2$, $\tilde{G} = G\,(\alpha)/r_0c^2$.
In the limiting case, for $\alpha = 1$, which corresponds to equality $c = c_e$, equations (A9) take the form defined by Hugoniot's relations at the jump: $U^e = \theta$, $S_r^e = \left(\tilde{K} + 4/3\tilde{G}\right)\theta = \frac{c_e^2}{c_2}\theta = \alpha^2\theta = \theta$.

References

1. Forrestal, M.J., Longcope, D.B.: Closed-form solution for forces on conical-nosed penetrators into geological targets with constant shear strength. Mech. Mater. **1**(4), 285–295 (1982)
2. Forrestal, M.J., Norwood, F.R., Longcope, D.B.: Penetration into targets described by locked hydrostats and shear strength. Int. J. Solids Structures. **17**(9), 915–924 (1981)
3. Forrestal, M.J., Luk, V.K.: Penetration into soil targets. Int. J. Impact. Eng. **12**(3), 427–444 (1992)
4. Forrestal, M.J., Luk, V.K.: Dynamic spherical cavity-expansion in a compressible elastic-plastic solid. Trans. ASME. J. Appl. Mech. **55**(2), 275–279 (1988)
5. Durban, D., Masri, R.: Dynamic spherical cavity expansion in a pressure sensitive elastoplastic medium. Int. J. Solids Structures. **41**(7), 5697–5716 (2004)
6. Meng, C., Tan, Q., Jiang, Z., Song, D., Liu, F.: Approximate solutions of finite dynamic spherical cavity-expansion models for penetration into elastically confined concrete targets. Int. J. Impact Eng. **114**, 182–193 (2018)
7. Cleja-Tigoiu, S., Cazacu, O., Tigoiu, V.: Dynamic expansion of spherical cavity within a rate-dependent compressible porous material. Int. J. Plasticity. **24**(5), 775–803 (2008)
8. Feng, J., Li, W.B., Wang, X.M., Song, M.L., Ren, H.Q., Li, W.B.: Dynamic spherical cavity expansion analysis of rate-dependent concrete material with scale effect. Int. J. Impact Eng. **84**, 24–37 (2015)
9. Rosenberg, Z., Dekel, E.: A numerical study of the cavity expansion process and its application to long-rod penetration mechanics. Int. J. Impact Eng. **35**(3), 147–154 (2008)
10. Rosenberg, Z., Dekel, E.: Analytical solution of the spherical cavity expansion process. Int. J. Impact Eng. **36**(2), 193–198 (2009)
11. Masri, R., Durban, D.: Deep penetration analysis with dynamic cylindrical cavitation fields. Int. J. Impact Eng. **36**(6), 830–841 (2009)
12. Masri, R., Durban, D.: Cylindrical cavity expansion in compressible Mises and Tresca solids. Euro. J. Mechanics A/Solids. **26**(4), 712–727 (2007)
13. Suzuki, Y., Lehane, B.M.: Analysis of CPT end resistance at variable penetration rates using the spherical cavity expansion method in normally consolidated soils. Comput. Geotechnics. **69**, 141–152 (2015)
14. Cheng, Y., Yang, H.-W., Sun, D.: Cavity expansion in unsaturated soils of finite radial extent. Comput. Geotechnics. **102**, 216–228 (2018)
15. Su, D., Yang, Z.X.: Drained analyses of cylindrical cavity expansion in sand incorporating a bounding-surface model with state-dependent dilatancy. Appl. Math. Model. **68**, 1–20 (2019)
16. Shi, C., Wang, M., Li, J., Li, M.: A model of depth calculation for projectile penetration into dry sand and comparison with experiments. Int. J. Impact Eng. **73**, 112–122 (2014)
17. Shi, C., Wang, M., Zhang, K., Cheng, Y., Zhang, X.: Semi-analytical model for rigid and erosive long rods penetration into sand with consideration of compressibility. Int. J. Impact Eng. **83**, 1–10 (2015)
18. Masri, R., Durban, D.: Dynamic Spherical Cavity Expansion in an Elastoplastic Compressible Mises Solid. ASME JAM **72**, 887–898 (2005). https://doi.org/10.1115/1.1985428
19. Cohen T., Masri R., Durban D.: Shock Waves in Dynamic Cavity Expansion. 2010, ASME JAM, 77, 041009-1-8 https://doi.org/10.1115/1.4000914
20. Cohen T., Durban D.: Hypervelocity Cavity Expansion in Porous Eiastopiastic Solids. 2013, ASME JAM, 80, 011017-1-7 https://doi.org/10.1115/1.4007224
21. Yu, H.-S.: Cavity Expansion Methods in Geomechanics. Kluwer, Dordrecht (2000)
22. Ben-Dor, G., Dubinsky, A., Elperin, T.: Applied High-Speed Plate Penetration Dynamics. Springer, Dordrecht (2006)
23. Ben-Dor, G., Dubinsky, A., Elperin, T.: Engineering models of high speed penetration into geological shields. Central Euro. J. Eng. **1**(4), 1–19 (2014)
24. Omidvar, M., Iskander, M., Bless, S.: Response of granular media to rapid penetration. Int. J. Impact Eng. **66**, 60–82 (2014)
25. Omidvar, M., Doreau-Malioche, J., Bless, S., Iskander, M.: Phenomenology of rapid projectile penetration into granular soils. Int. J. Impact Eng. **85**, 146–160 (2015)
26. Forrestal, M.J., Tzou, D.Y., Askari, E., Longcope, D.B.: Penetration into ductile metal targets with rigid spherical-nose rods. Int. J. Impact Eng. **16**(5/6), 699–710 (1995)
27. Chen, X.W., Li, Q.M.: Deep penetration of a non-deformable projectile with different geometrical characteristics. Int. J. Impact Eng. **27**(6), 619–637 (2002)
28. Forrestal, M.J., Warren, T.L.: Penetration equations for ogive-nose rods into aluminum targets. Int. J. Impact Eng. **35**(8), 727–730 (2008)
29. Warren, T.L.: The effect of target inertia on the penetration of aluminum targets by rigid ogive-nosed projectiles. Int. J. Impact Eng. **91**, 6–13 (2016)
30. Rosenberg, Z., Dekel, E.: A comment on "The effect of target inertia on the penetration of aluminum targets by rigid ogive-nosed long rods" by T.L. Warren Int. J. Impact Eng. 2016, Int. J. Impact Eng. **93**, 231–233 (2016)

31. Warren, T.L.: Response to: A comment on "The effect of target inertia on the penetration of aluminum targets by rigid ogive-nosed long rods" by T.L. Warren, Int. J. Impact Eng. 2016 by Z. Rosenberg and E. Dekel. Int. J. Impact Eng. **93**, 234–235 (2016)
32. Kong, X.Z., Wu, H., Fang, Q., Peng, Y.: Rigid and eroding projectile penetration into concrete targets based on an extended dynamic cavity expansion model. Int. J. Impact Eng. **100**, 13–22 (2017)
33. Rosenberg, Z., Kositski, R., Dekel, E.: Comment on: "Rigid and eroding projectile penetration into concrete targets based on an extended dynamic cavity expansion model" by Kong et al. Int. J. Impact Eng. (2017), Int. J. Impact Eng. **104**, A1–A3 (2017)
34. Kong, X.Z., Wu, H., Fang, Q., Peng, Y.: Response to: Comment on "Rigid and eroding projectile penetration into concrete targets based on an extended dynamic cavity expansion model" by Kong et al. Int. J. Impact Eng. 2017 by Z. Rosenberg et al. Int. J. Impact Eng. **104**, 150–153 (2017)
35. Warren, T.L., Hanchak, S.J., Poormon, K.L.: Penetration of limestone targets by ogive-nosed VAR 4340 steel projectiles at oblique angles: experiments and simulations. Int. J. Impact Eng. **30**(10), 1307–1331 (2004)
36. Warren, T.L.: Simulations of the penetration of limestone targets by ogive-nose 4340 steel projectiles. Int. J. Impact Eng. **27**(5), 475–496 (2002)
37. Li, Q.M., Flores-Johnson, E.A.: Hard projectile penetration and trajectory stability. Int. J. Impact Eng. **38**(10), 815–823 (2011)
38. Sun, Q., Sun, Y., Liu, Y., Li, R., Zhao, Y.: Numerical analysis of the trajectory stability and penetration ability of different lateral-abnormal projectiles for non-normal penetration into soil based on Modified Integrated Force Law method. Int. J. Impact Eng. **103**, 159–168 (2017)
39. Kotov, V.L., Balandin, V.V., Bragov, A.M., Linnik, EYu., Balandin, V.V.: Using a local-interaction model to determine the resistance to penetration of projectiles into sandy soil. J. Appl. Mech. Tech. Phys. **54**(4), 612–621 (2013)
40. Bazhenov, V.G., Balandin, V.V., Grigoryan, S.S., Kotov, V.L.: Analysis of models for calculating the motion of solids of revolution of minimum resistance in soil media. J. Appl. Math.Mech. **78**(1), 65–76 (2014)
41. Balandin, Vl.V., Balandin, Vl.Vl., Bragov, A.M., Kotov, V.L.: Experimental study of the dynamics of penetration of a solid body into a soil medium. Tech. Phys. **61**(6), 860–868 (2016)
42. Kotov, V.L., Balandin, V.V., Bragov, A.M., Balandin, Vl.Vl.: Investigation of dynamic resistance to the shear of water-saturated sand according to the results of the Inverse Experiment Technique. Technical Physics Letters. **43**(9), 808–810 (2017)
43. Bragov, A.M., Balandin, Vl.V., Kotov, V.L., Balandin, Vl.Vl.: Investigation of the dynamic properties of water-saturated sand by the results of inverted experiments. Tech. Phys. **63**(4), 530–539 (2018)
44. Bragov, A.M., Balandin, V.V., Igumnov, L.A., Kotov, V.L., Kruszka, L., Lomunov, A.K.: Impact and penetration of cylindrical bodies into dry and water-saturated sand. Int. J. Impact Eng. **122**, 197–208 (2018)
45. Lyakhov, G.M.: Shock waves in soil and water sand dilution. (in Rus.). Zh. Prikl. Mekh. Tekhn. Fiz. **2**(1), 38–46. [English translation in: J. Appl. Mech. Tech. Phys.] (1961)
46. Lyakhov, G.M.: Experimental study of blast waves in clayey soil. (in Rus.). Zh. Prikl. Mekh. Tekhn. Fiz. **2**(2), 123–126 (1961)
47. Rykov, G.V.: Experimental study of stress field in an explosion in sandy soil. (in Rus.). Zh. Prikl. Mekh. Tekhn. Fiz. **5**(1), 85–89 (1964)
48. Lagunov, V.A., Stepanov, V.A.: Measurements of the dynamic compressibility of sand under high pressures. (in Rus.). Zh. Prikl. Mekh. Tekhn. Fiz. **4**(1), 88–96 (1963)
49. Arlery, M., Gardou, M., Fleureau, J.M., Mariotti, C.: Dynamic behaviour of dry and water-saturated sand under planar shock conditions. Int. J. Impact Eng. **37**(1), 1–10 (2010)
50. Kinslow, R.: High-Velocity Impact Phenomena. Academic Press, New York, London (1970)
51. Bragov, A.M., Lomunov, A.K., Sergeichev, I.V., Proud, W., Tsembelis, K., Church, P.: A Method for Determining the Main Mechanical Properties of Soft Soils at High Strain Rates (103–105s-1) and Load Amplitudes up to Several Gigapascals. Tech. Phys. Letters. **31**(6), 530–531 (2005)
52. Jeanloz, R.: Shock wave equation of state and finite strain theory. J. Geophys. Res. **94**, 5873–5886 (1989)
53. Bazhenov, V.G., Bragov, A.M., Kotov, V.L., Kochetkov, A.V.: An investigation of the impact and penetration of solids of revolution into soft earth. J. Appl. Math. Mech. **67**(4), 611–620 (2003)
54. Bazhenov, V.G., Kotov, V.L., Kochetkov, A.V., Krylov, S.V., Feldgun, V.R.: On wave processes in soil subjected to a surface charge explosion. Mech. Solids. **36**(2), 62–68 (2001)
55. Forrestal, M.J., Longcope, D.B.: Target strength of ceramic materials for high velocity penetration. J. Appl. Phys. **67**, 3669–3672 (1990)
56. Proud, W.G., Chapman, D.J., Williamson, D.M., Tsembelis, K., Addiss, J., Bragov, A., Lomunov, A., Cullis, I.G., Church, P.D., Gould, P., Porter, D., Cogar, J.R., Borg, J.: The dynamic compaction of sand and related porous systems // "Shock Compression of Condensed Matter"—2007: Proceedings of the Conference of the American Physical Society Topical Group on Shock Compression of Condensed Matter. AIP Conference Proceedings. **955**, 1403-1408 https://doi.org/10.1063/1.2832988 (2007)
57. Linnik, EYu., Kotov, V.L., Tarasova, A.A., Gonik, E.G.: The solution of the problem of the expansion of a spherical cavity in a soil medium assuming incompressibility beyond the shock front. (in Rus.). Problems of Strength and Plasticity. **74**, 49–58 (2012)
58. Allen, W.A., Mayfield, E.B., Morrison, H.L.: Dynamics of a projectile penetrating sand. J. Appl. Phys. **28**(3), 370–376 (1957)